

AIR MASS MODIFICATION OVER THE GULF OF ST. LAWRENCE

by

P.L.J. Morin

A thesis submitted to the Faculty of Graduate Studies  
and Research in partial fulfilment of the requirements  
for the degree of Master of Science.

Department of Meteorology  
McGill University  
Montréal, Canada

July, 1973

ABSTRACT

A model is developed for the computation of meteorological parameters required for determining the turbulent fluxes of moisture and heat over the Gulf of St. Lawrence.

The air-sea interaction of air masses moving over the Gulf is examined.

It is shown that estimates of the advection of sensible and latent heat is best obtained from an energy budget analysis of sensible heat and moisture.

## RESUME

Un modèle est construit qui détermine les paramètres essentiels pour calculer les fluxes de la chaleur sensible et de l'humidité au dessus du Golfe du St. Laurent.

L'interaction entre la masse d'eau et les masses d'air qui traversent le Golfe est examinée.

Il est démontré que la détermination de l'advection de la chaleur sensible et de l'humidité peut être accomplie par l'analyse du bilan énergétique de la chaleur sensible et de l'humidité.

## ACKNOWLEDGEMENTS

The author is indebted to a number of people and agencies for their contributions to the present work. The Atmospheric Environment Services of Canada provided financial support. Dr. E. Vovinckel, the author's advisor, and Dr. Svann Orvig for their constant source of help and encouragement. The Canadian Meteorological Center of Montréal who provided the assistance and facilities in acquiring the data. Mrs. C. Chouinard for preparing the typescript. I am inexpressibly grateful to my wife Donna for her encouragement and help in my work, all the while supporting 2 sons - one of which will be forever remembered by this work.

## TABLE OF CONTENTS

	Page
Abstract	i
Resumé	ii
Acknowledgements	iii
List of Figures	vi
List of Tables	viii
CHAPTER I INTRODUCTION	1
CHAPTER II ENERGY AND WATER BUDGET OF AN AIR COLUMN	2
2.1 Sensible Heat Budget Equation	2
2.2 Latent Heat Budget Equation	3
2.3 Radiative Terms	3
2.3.1 Short Wave Radiation	4
2.3.2 Long Wave Radiation	4
2.4 Latent and Sensible Heat Terms	7
2.5 Advective Terms	8
2.6 Precipitation	10
CHAPTER III FORMATION OF THE METEOROLOGICAL FIELDS	11
3.1 Initialization	11
3.1.1 Interpolation	11
3.1.2 Temperature and Moisture Fields	12
3.1.3 Pressure and Wind Fields	14
3.1.4 Accuracy of Interpolated Temperature and Moisture Fields	17
3.2 Latent and Sensible Heat Fluxes	20
3.3 Behaviour of Radiative terms to Meteorological Parameter Changes	23
3.3.1 Short Wave Radiation	26
3.3.2 Long Wave Radiation	27

CHAPTER III (continued)	Page
3.3.3 Heating Rate	33
3.4 Nephanalysis	33
3.5 Air Mass Transformation - Model	36
3.5.1 Advection of Air Parcels	36
3.5.2 Sensible Heat Distribution	37
3.5.3 Latent Heat Distribution	38
3.5.4 Islands	39
3.5.5 Interface Temperature	39
3.6 Water-Body Model	39
CHAPTER IV APPLICATION OF THE MODEL	41
4.1 Advection of an Air Column	41
4.2 Air Mass Transformation Over the Gulf Region	46
4.3 Verification	55
4.3.1 Modification of Shore Line Profiles	56
4.3.2 Water-Body Heat Content	61
4.4 Summary	63
4.5 Water and Energy Budget Analysis	63
4.5.1 Precipitation	64
4.5.2 Storage Terms	64
4.5.3 Latent and Sensible Heat Terms	66
4.5.4 Radiative Terms	67
4.5.5 Advective Terms	67
4.5.6 Energy Disposition	69
CHAPTER V CONCLUSION	71
APPENDIX A DESCRIPTION OF WATER BODY PROCESSES (LALLY, 1973)	72
BIBLIOGRAPHY	77

## LIST OF FIGURES

Figure		Page
1	Short Wave Radiation Absorbed as a Function of Cloud Area and Thickness	5
2	Gulf of St. Lawrence with Grid Overlay	13
3	Sensible Heat Exchange and Air-Sea Temperature Difference as a Function of Wind Speed	19
4	Sensible and Latent Heat Fluxes for Three Different Speeds	21
5	Temperature and Moisture Soundings for two Reporting Stations	22
6	Latent and Sensible Heat Fluxes Over Varying Ice Surfaces	24
7	Latent and Sensible Heat Fluxes Over Varying Ice Surfaces	25
8	Long Wave Radiation as a Function of Cloud Amount and Height	28
9	Long Wave Radiation as a Function of Air Mass Modification	30
10	Cloud Amount as a Function of the Relative Humidity	35
11	Temperature Profiles of an Advected Parcel	42
12	Moisture Profiles of an Advected Parcel	43
13	Cloud Profile Along Various Points of the Path of Motion	44
14	Mean Sea Level Pressure Pattern and Wind Field for Five Synoptic Situations	47
15	Transformed Temperature Field and Changes (Dec. 29, 1971)	48

Figure		Page
16	Transformed Moisture Field and Changes (Dec. 29, 1971).	49
17a	Interpolated Temperature and Moisture Fields (Feb. 4, 1972)	51
17b	Polygon Enclosing Area Used for Calculating Advection of Fluxes	51
18	Transformed Temperature Field and Changes (Feb. 4, 1972)	52
19	Transformed Moisture Field and Changes (Feb. 4, 1972)	53
20	Actual Reported Ice Field and the Corresponding Computer Produced Ice Field	54
21	Shore-Line Temperature and Moisture Profile (Dec. 23, 1971)	57
22	Shore-Line Temperature and Moisture Profile (Dec. 29, 1971)	58
23	Shore-Line Temperature and Moisture Profile (Feb. 2, 1972)	59
24	Water Body Heat Loss at Four Water Grid Points	62

LIST OF TABLES

TABLE		PAGE
1	Isobaric Levels of Available (X) and Interpolated (I) Data	14
2	Changes in Long Wave Radiation as a Function of Temperature and Moisture Changes	26
3	Components of the Sensible Heat and Moisture Budget Equations	65
4	Components of the Sensible Heat Budget	70

## CHAPTER I

## INTRODUCTION

The purpose of this study is to determine the effect exerted by a small water-ice body on the water and energy budgets of traversing air masses. The feasibility of estimating the water and sensible heat gains from geostrophic fluxes and from the balance of energy and water budgets is also examined. Bradbury (1957), Estoque and Benton (1954), Manabe (1967), Ninomiya (1968,1972), and Palmén and Soderman (1966), are among some of the numerous authors who have investigated water and energy budgets over land and water surfaces. Burbidge (1951), Burke (1945), and Craddock (1951) examined the transformation of individual air parcels traversing water bodies. Coombs (1962), Danielson (1969), and Matheson (1967) examined energy budgets over water bodies and correlated flux exchanges averaged over a time period of ice formation.

To the author's knowledge, no attempt has been made to combine an atmospheric model with water-body and surface energy budget models, using twice-daily meteorological information to estimate water and sensible flux exchanges for periods prior to and during ice formation over an area covered by a large annual ice field. The steps necessary in the solution for the region of the Gulf of St. Lawrence were:

1. constructing initial fields of temperature, humidity, and cloud for the Gulf and surrounding regions every 12 hours.
2. determining the effect of various meteorological parameters on the moisture and sensible heat fluxes.
3. modifying the low level profiles of various meteorological parameters, using a computer model.
4. applying the redefined meteorological fields in estimating energy exchanges, and determining the energy budget of the Gulf through the use of a water-ice body model.

## CHAPTER II

## ENERGY AND WATER BUDGET OF AN AIR COLUMN

2.1 Sensible Heat Budget Equation

The change in sensible heat in a given atmospheric column can be represented by

$$\Delta SH = QR + QD + QS + QSADV + PCPN \quad (1)$$

where  $QR$  = net change in sensible heat attributable to long and short wave radiation.

$QD$  = net change of sensible heat from dynamic process such as subsidence. Craddock (1951) in his analysis of air mass transformation considered it negligible.

$QS$  = change in sensible heat resulting from vertical transfer of sensible heat at the base of the column.

$QSADV$  = sensible heat changes resulting from advection <sup>of</sup> air parcels across the column walls. The sensible heat of an advected air column consists of the sensible heat associated with the three components making up the air column: dry air, water vapor, and the liquid water of clouds.

$PCPN$  = sensible heat gain due to precipitation, that is,  $PCPN = L \cdot R$  where  $L$  is the latent heat of sublimation or vaporization and  $R$  is the water equivalent of the precipitation recorded.

If cloud formation and dissipation occurs in a given air column, it can be considered a reversible process as it does not affect the total water or sensible heat content of the column. On the other hand, precipitation or cloud leaving a column reduces the water content of the column. The latent heat release associated with precipitation will increase the sensible heat of the column. However, the sensible heat gain from cloud formation and subsequent departure from the column, will raise the temperature field (close to the cloud and generally moving) with the cloud field.

This will result in a slight error if such transport of cloud as well as other discontinuities in the fields fail to be recorded at the column walls due to the distance between reporting stations.

## 2.2 Water Budget Equation

The change in the moisture content in a given vertical column is given by

$$\Delta LH = QE + QEADV - PCPN \quad (2)$$

where  $QE$  = net gain in moisture resulting from the vertical transfer of latent heat at the base of the air column. A minor component is the latent heat exchange associated with evaporating precipitation which can be neglected when compared to the major component of  $QE$ .

$QEADV$  = moisture change associated with the advection of clouds and water vapor through the column walls.

$PCPN$  = moisture lost by precipitation leaving the column.

The breakdown of the budget equation into various measurable terms allows one to calculate the flux contributions of the various interacting terms. The theoretical background for the necessary calculations will be discussed in following sections.

## 2.3 Radiative Terms

The net change in sensible heat in an atmospheric column, attributable to long and short wave radiation is given by:

$$QR = SAA + RLU - DFL - UFL \quad (3)$$

where  $SAA$  = short wave radiation absorbed in the atmosphere,

$RLU$  = long wave radiation emitted from the earth's surface and absorbed in the atmosphere,

$DFL$  = long wave radiation emitted from the atmosphere to the earth's surface,

UFL = long wave radiation from the atmosphere lost to outer space.

### 2.3.1 Short Wave Radiation

The short wave radiation absorbed by an air column will be the result of several processes occurring during its transit: absorption by various gases and clouds, and scattering by dry air, dust particles, and clouds. The model used in calculating the short wave radiation absorbed by the atmosphere (SAA) is one designed by Woinckel and Orvig (1972). Figure 1 illustrates the amount of short wave radiation absorbed by the atmosphere (SAA) for various amount of cloud cover and thickness as calculated by the model for a particular day. The isobaric levels of the cloud base and cloud top of a particular cloud layer are denoted by the ends of the vertical columns of figure 1. The term SAA is about 15% of the short wave radiation penetrating the 300 mb level of the atmosphere. A change from near clear sky conditions to an almost overcast condition throughout the atmosphere results in an 8% decrease of the short wave radiation reaching the earth's surface, and an increase of about 25% in SAA. The contribution of SAA to the sensible heat is generally one order of magnitude less than the gains attributable to latent and sensible heat exchanges at the interface. The expected errors in cloud amount and thickness will not affect significantly the short wave heat budget term of an atmospheric column.

### 2.3.2 Long Wave Radiator

The change in the radiation intensity for a monochromatic beam penetrating a thin layer of gas is given by Schwarzschild's equation of radiative transfer:

$$dI_{\lambda} = K_{\lambda} \cdot \rho \cdot ds \cdot (f(\lambda, T) - I_{\lambda})$$

where  $K_{\lambda}$  = absorption coefficient of the gas,

$\rho$  = density of the gas,

$ds$  = thickness of the gas layer,

$f(\lambda, T)$  = Planck black body emission rate,

$I_{\lambda}$  = intensity of incident beam.

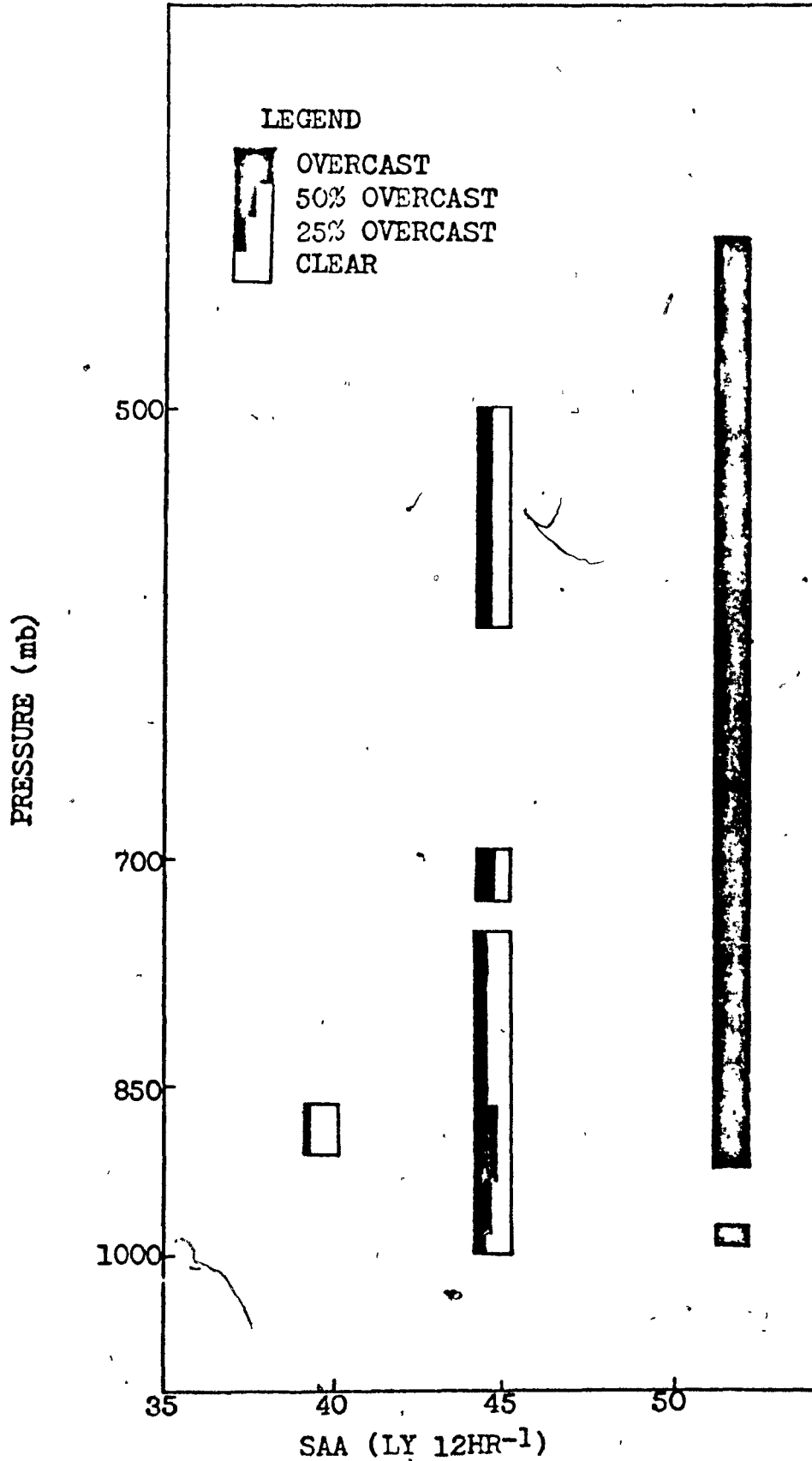


Fig. 1 Short wave radiation absorbed as a function of cloud area and thickness.

The computation of the radiation fluxes  $F$  for the atmosphere having varying absorbing gases and temperatures requires solving the radiative transfer equation (Elsasser and Culbertson, 1960):

$$F = \int d_{\nu} \int_{u_0}^{u_1} B_{\nu}(T(u)) \tau_f \left[ \frac{\partial L_{\nu}(T)(u-u_0)}{\partial u} \right] du \quad (5)$$

where  $B_{\nu}$  = monochromatic hemispheric black body flux,  
 $\tau_f$  = flux transmission function,  
 $L$  = generalized absorption coefficient,  
 $T$  = temperature ( $^{\circ}K$ ),  
 $u$  = optical path length of the radiation gas,  
 $\nu$  = wave number.

Because of the varying nature of  $\tau_f$  with frequency, the exact solution of the above equation is virtually impossible. Several alternative methods exist in calculating long wave radiation absorption and distribution.

A simple method utilizes empirical formulas which incorporate observed surface parameters such as temperature, pressure, humidity, and cloud cover and type. Zillman (1972) gives a summary of such formulas. A more complex and accurate method incorporates the vertical profiles of temperature, moisture, carbon dioxide and cloud amount and thickness. Elsasser (1942), Kondrat'yev (1969) and Yamamoto (1952) have developed schemes that will allow the use of such profiles.

The model used by the author is one developed by Vowinckel and Orvig (1972) which calculates long wave radiation transmitted and absorbed, based on studies of Kondrat'yev (1969). This model treats each cloud layer as a black body. The radiative temperature of the cloud top or base is coincident with an atmospheric level. The long wave radiation transferred through each level and lost to space (UFL) or emitted to the ground (DFL) is estimated. The radiation emitted by a cloud surface is proportional to the four power of its temperature. Because of the steep lapse rate in the lower atmosphere, it is essential to have accurate temperature and height estimates of cloud tops and bases. An atmosphere subdivided into several layers is therefore essential in order to depict accurately cloud bases, tops, and cloud surface temperatures. Since the temperature lapse rate is steeper in the lower

atmosphere than the near isothermal conditions in the lower stratosphere, a larger number of layers is desirable in the lower atmosphere. Temperature and moisture profiles are available on a routine basis for certain isobaric levels. The required intermediate temperature and moisture profiles provided through interpolation techniques will not depict the true state accurately. Similarly, cloud profiles generated by interpolating surface cloud observations will have errors. Using only the six significant isobaric levels would not be sufficiently accurate. On the other hand, using a model with a large number of levels would be too costly. The model used in the present study has seventeen levels with eleven levels occurring below the 500 mb level. The long wave radiation, as computed by the model, will be significantly better than that derived from the simple empirical methods.

The long wave radiation emitted from the underlying surface is approximated by the Stephan-Boltzman law:  $RLU = \sigma \cdot T^4 \cdot \epsilon$

where  $\sigma$  = Stephan-Boltzman constant,

$T$  = underlying surface temperature,

$\epsilon$  = emissivity.

#### 2.4 Latent and Sensible Heat Terms

Several methods exist for calculating latent and sensible heat fluxes. A direct method is the measurement of eddy fluxes by the eddy correlation technique, which requires on-site measurements with extensive instrumentation.

Another method involves the use of the Bowen Ratio, that is  $QE = K \cdot QS$  where  $K$  is a function of the air-sea temperature difference, vapor pressure difference, and the reference level of temperature and humidity. The parameter  $K$ , as determined from actual measurements for given synoptic situations over certain geographical areas is utilized in analogous situations where either  $QE$  or  $QS$  is known. Because each synoptic situation is characterized by its own temperature and humidity profiles,  $K$  will vary for similar situations. In situations of weak temperature and humidity gradients, this method will often give not only incorrect scalar values, but also an incorrect direction of flux exchange. In the area under study no distribution pattern of  $QE$  or  $QS$  is available to allow the use of the Bowen ratio.

The method most widely adopted uses equations for QE and QS as developed from hydrodynamic analysis:

$$\begin{aligned} QS &= -\rho \cdot c_p \cdot K_s \cdot \partial\theta/\partial Z = c_p \cdot \rho \cdot C_A \cdot (\bar{\theta}_0 - \bar{\theta}_a) \cdot \bar{u}_a \\ QE &= \rho \cdot K_e \cdot \partial q/\partial Z = \rho \cdot C_A \cdot (\bar{q}_0 - \bar{q}_a) \cdot \bar{u}_a \end{aligned} \quad (6)$$

where  $K_s$ ,  $K_e$  = exchange coefficient of heat and moisture respectively,

$\rho$  = air density,

$\theta_a$ ,  $\theta_0$  = potential temperature at height  $Z = a$  and  $Z = 0$  respectively,

$q_a$ ,  $q_0$  = vapor pressure at height  $Z = a$  and  $Z = 0$  respectively,

$u_a$  = mean velocity at height  $Z = a$ ;  $u_0$  is assumed zero at the surface,

$C_A$  = proportionately constant,

$c_p$  = heat capacity for dry air.

The above equations serve as a first approximation only, due to the following five shortcomings. First, they are valid for infinite homogeneous surfaces. Second, the exchange coefficients are greatly dependent on thermal stability, wind shear, and the roughness of the underlying surface. Furthermore, as shown by many authors and summarized by Munn (1964), the exchange coefficient varies with the parameter under transport by turbulence. In this work the formula used is one developed by Vowinckel and Orvig (1972), the term  $C_A$  accounts for the vertical thermal stability at the interface.

Since synoptic scale processes are the main factors determining QE and QS, their calculation should be made over a sufficiently short time step in relation to the cycle time of synoptic events - usually 2 to 3 days. In this study, the time resolution was limited to 12 hours - the time between available upper air data reports. Vowinckel (1965), in his analysis of energy budgets over the North Atlantic, discusses the frequency of observation with the representativeness of the observed parameter over a time period and concludes that "main pulsations of evaporation are reasonably well sampled with 2 observations per day".

## 2.5 Advective Terms

Between any two levels of the atmosphere, the advection of sensible

heat and moisture through a vertical column wall may be expressed by the following equations:

$$QSADV = TM*(C_p + SHHM*C_v + FLWC*C_w)*FX$$

$$QEADV = (SHHM + FLWC)*L*.001*FX \quad (7)$$

where TM = mean layer temperature ( $^{\circ}K$ )

SHHM = mean layer specific humidity ( $g\ kg^{-1}$ )

FLWC = mean liquid water content of the layer ( $g\ kg^{-1}$ )

CLWC = cloud water content ( $g\ kg^{-1}$ )

L = latent heat of vaporization

$C_p$ ,  $C_v$ ,  $C_w$  = heat capacity of dry air, water vapor, and liquid water respectively

FX = product of wind and the isobaric mass between 2 isobaric levels

.001 = normalization factor as moisture is expressed in grams per kilogram of dry air.

In any given layer, the mass of water vapor is

$$SHHM = \int_{P_{i-1}}^{P_i} \left( \frac{\rho_w}{\rho} \right) \cdot \frac{dp}{g}$$

where  $\rho_w/\rho$  = specific humidity distribution,

g = acceleration due to gravity,

dp = pressure increment.

Because the moisture content of the atmosphere is generally small for the region under study, the error in replacing the specific humidity with the mixing ratio is well within the error range of reported humidities. Similarly, the use of  $1000\ cm\ s^{-2}$  for "g" instead of  $980\ cm\ s^{-2}$  is again negligible and the "g" term can be included implicitly in the isobaric mass expressed in mb.

An ideal measurement of sensible heat and water fluxes through a column wall would require continuous temperature, humidity, cloud, and wind profiles. Since the data were available only for every 12 hours, and only for certain isobaric levels from surrounding Gulf Stations, a

continuous time and space profile is not available.

## 2.6 Precipitation - PCPN

With a knowledge of precipitation distribution, an estimate of latent heat release is possible. Again, depending on the type of synoptic situation, the contribution of PCPN to the energy budget equations may vary from nil to several times the amount of solar radiation reaching the upper atmosphere.

Since precipitation amounts and type are most difficult to estimate over water regions, the contribution of PCPN to the budget equations can lead to large errors for two main reasons. First, the area of precipitation associated with cyclonic situations will cover extensive areas and will seldom be influenced by the underlying surface. The precipitation field will be adequately recorded by the meteorological station. A precipitation field derived from numerical analysis of shore based data points would be reasonably accurate. However, in anticyclonic cases characterized by polar outbreaks, areas such as the Gulf will give rise to rapid destabilization of the air mass and enhance precipitation near off-shore regions. Interpolation of only shore based data will therefore tend to underestimate distribution and total precipitation. Second, latent heat release from 1 gram of liquid and solid precipitation is approximately 600 and 680 cal gm<sup>-1</sup> respectively. A 13% variation in the estimate of latent heat release is possible as only on-site observations can determine the type of precipitation. During the winter season examining surface temperatures is inadequate as precipitation will frequently penetrate an upper air inversion, whose temperature is higher than 0°C, and reach the interface in liquid form after penetrating a lower level cold air layer whose temperature may be several degrees below zero. A third source of error is the presence of errors in the reported data. In this study, a precipitation field was obtained by a numerical analysis of data from reporting stations around the Gulf area.

## CHAPTER III

## FORMATION OF THE METEOROLOGICAL FIELDS

3.1 Initialization

The aim of this section is to discuss the generation of horizontal and vertical temperature, humidity, and cloud fields required in studying the energy and water budgets for the area in question.

The representativeness of coastal points for over-water vertical profiles is greatly dependent on the type of synoptic situation. A strong subsiding high-pressure area in which the air temperature is greater than that of the water body would experience little modification. Emmons (1947) found the thickness of the modified layer to be only 180 meters thick after a trajectory of 300 miles, where the wind was less than  $8 \text{ m s}^{-1}$  and the air temperature exceeded the water temperature by 5 deg. to 10 deg. C. At the other extreme, heating of cold polar air by warm water bodies is so representative of over-water profiles (Burke, 1945; Burbidge, 1951). Windward coast profiles however, would still be fairly representative for regions near the shore and under the same streamline flow.

The following sections discuss the construction of temperature, humidity, and cloud profiles using meteorological data, and the sensitivity of the radiation budget terms to changes in these derived fields.

3.1.1 Interpolation

The technique used for numerical analysis of fields is the one developed by Gandin (1965). It differs from linear interpolation in that the weight function is an exponential decrease from data point to grid point rather than a linear function of their separation. This results in data points, nearest the grid point being evaluated, having a very strong influence on the final grid point value. The quality of the final analysis is dependent on the density of the observation network. In a numerical analysis of a high density area of reporting stations, INTER, the subroutine which numerically analyses the field, would be used to filter out errors

rather than simply construct a field.

In reality the area under study, figure 2, has only 2 radiosondes and 8 synoptic stations along the shores of the area. All other reports are from surrounding land stations which include about 19 synoptic stations and 3 additional radiosonde stations. Land-based stations are influenced to some extent by local topographical features, and some reported meteorological parameters may be highly influenced. Depending on the particular parameter being analysed, the resulting field may serve as an initial first guess or as a final field for calculating energy budgets. The following sections discuss which parameters are assumed representative, and which must be redefined.

### 3.1.2 Temperature and Moisture Fields

This section discusses the formation of temperature and specific humidity fields. The required data for the reporting stations shown in figure 2 were extracted from history tapes kindly supplied by the Atmospheric Environment Service of Canada.

The surface data from radiosondes and synoptic stations consisted of pressure, temperature, dew point, cloud type and amounts, precipitation, visibility and weather type. Missing surface data were retrieved from surface synoptic maps whenever possible. The upper air data consisted of temperature and dew points for the significant isobaric levels - 850, 700, 500, 300, 150 mb. The vertical temperature and moisture profiles have been checked previously for consistency. Whenever possible, missing upper air values were retrieved from Canadian Upper Air Data Bulletin.

As the recording radiosonde element for moisture is unreliable above the 400 mb level, the dew point is not available. As there exists little climatological data for water vapor above 400 mb, the atmosphere was assumed to be almost homogeneous with respect to water vapor. The dew points for the 150 mb and 300 mb levels were obtained by subtracting the 500 mb dew point difference from the reported temperature at 150 and 300 mb. This usually gave a value of mixing ratio from .001 to .05 g kg<sup>-1</sup>. Measurements by Mastenbrook (1966) indicated a mixing ratio of about .002 g kg<sup>-1</sup> above 400 mb the isobaric mass of moisture is negligible in both cases and the use

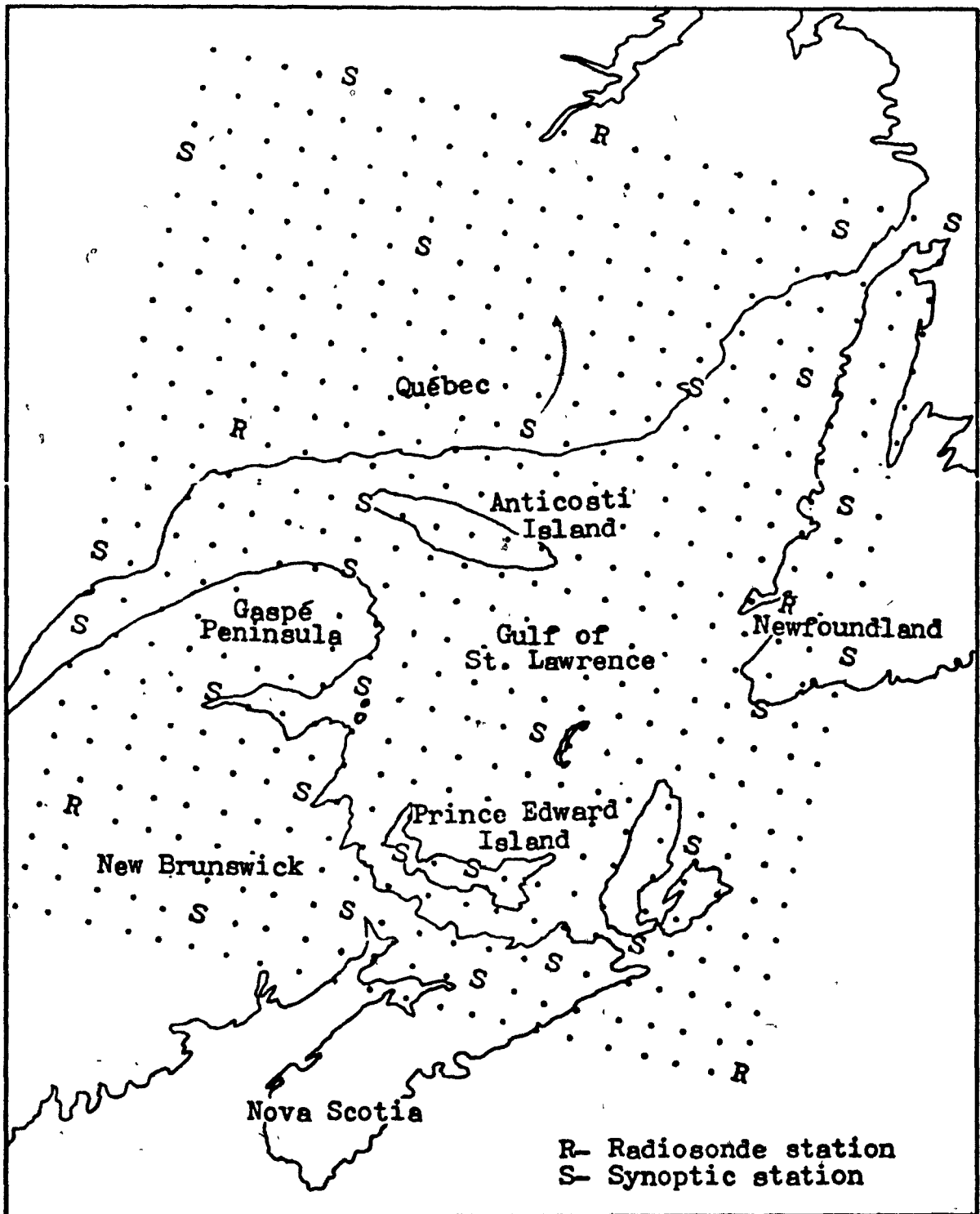


Fig. 2 Gulf of St. Lawrence with a grid overlay and grid positions of reporting stations.

of either value will have little effect on long wave radiation which, in the energy budget, is the term most sensitive to moisture changes.

A numerical analysis is performed on the temperature for the significant levels to yield a continuous horizontal temperature field over the grid area (figure 2). Similarly, after the dew points have been converted to specific humidities, a numerical analysis is performed to give a continuous moisture field over all grid points. As previously discussed, an atmosphere subdivided into several layers is essential in achieving an accurate estimate of long wave radiation fluxes. The subroutine "HUMPRO" linearly interpolates the humidity and temperature to produce a vertical profile of temperature and moisture for an additional 11 levels for each grid point (see Table 1). The subroutine "HEIGHT" later generates the height field for the significant isobaric levels from the temperature field. Clbud analysis executed by subroutine "ZNEPHE" uses the dew point field.

TABLE 1

ISOBARIC LEVELS OF AVAILABLE (X) AND INTERPOLATED (I) DATA

PRESSURE-P  
TEMPERATURE-TN  
DEW POINT TEMPERATURE-TD

TN	X	X	I	X	I	X	I	I	I	I	X	I	I	I	I	X
TD	I	I	I	X	I	X	I	I	I	I	X	I	I	I	I	X
P	150	300	400	500	600	700	730	760	790	820	850	I	I	I	I	X

### 3.1.3 Pressure and Wind Field

While surface wind reports are available, local topographical features seriously hamper their validity. Since a wind field generated from the surface pressure gradient is a better estimate of the actual wind, surface pressure reports were screened in an attempt to generate an accurate wind field.

The subroutine "CKPRGR" examines all reported pressures to detect possible transmission errors. Examination of synoptic maps revealed that the pressure gradient, over the grid area involved, seldom exceeded 44 mbs.

Thus, any pressure which departed from the mean pressure by 22 mbs was eliminated.

Numerous occasions arose when a reported pressure was a few mb above or below that of immediately surrounding data points. This type of error was most likely due to transmission difficulties. To prevent the generation of spurious winds, the data point was compared to the surrounding reported pressures, to determine its consistency with the surrounding field. The comparison was achieved by calculating the mean pressure gradient about all the reported data points and eliminating those data points whose pressure gradient exceeded the mean pressure gradient of all points by more than 90%. Once the final interpolated pressure field was obtained, the geostrophic wind field was computed using the geostrophic wind equation in the subroutine "WND." For levels in the lower atmosphere, the surface wind gradually approaches the geostrophic wind, usually at a height between 1000 and 2000 m depending on the synoptic situation and the terrain of the underlying surface. Roll (1965) describes several methods of determining the wind profile. As these methods require knowledge of vertical stability in the lowest 500 meters, with considerable accuracy, the methods were not utilized. From North Sea studies, Jeffreys (1920) arrived at a mean veer of  $16.5^\circ$  between the surface wind and the geostrophic wind while Reynolds (1956) obtained an average value between  $20^\circ$  and  $26^\circ$  for winds greater than 20 knots. Since the wind shear is a function of vertical stability -  $\frac{\partial T}{\partial Z}$  - and the horizontal gradient -  $\frac{\partial T}{\partial X}$ ,  $\frac{\partial T}{\partial Y}$  - of the temperature field (equation 8), lack of resolution led the author to assume a mean veer of  $8^\circ$  (the mean between  $0^\circ$  at the geostrophic and  $16^\circ$  at the surface) for all regions below the geostrophic level (Frost, 1948).

$$v_z = v_o + \int_{z=0}^z \frac{g}{ft} \frac{\partial T}{\partial X} dz + \int_{z=0}^z \frac{v}{T} \frac{\partial T}{\partial Z} dz \quad (8)$$

$$u_z = u_o + \int_{z=0}^z \frac{g}{ft} \frac{\partial T}{\partial Y} dz + \int_{z=0}^z \frac{u}{T} \frac{\partial T}{\partial Z} dz$$

Various findings on the ratio of surface wind ( $U_s$ ) to the geostrophic wind ( $U_g$ ), summarized by Roll (1965), indicate  $U_s * U_g^{-1}$  varies from .55 to .8 with the overall mean at .7. For levels above the laminar layer,

i.e. 50 to 100 meters above the interface, the wind is greater. Again, vertical stability is a strong factor in determining surface wind speed. In the shallow layer next to the surface, where maximum rates of latent and sensible heat exchanges occur, the surface wind chosen was  $.7*U_g$ . Since the period under study extended during the winter season, the unstable conditions over the Gulf could result in a higher mean value than .7. For the region above the laminar layer, the wind was taken to be  $.8*U_g$ .

In projecting vertical air columns extending from the surface to the geostrophic level for a time period during which the meteorological parameters do not change appreciably one could, in the mean, determine the streamline flow reasonably well using a speed equal to .9 of the geostrophic velocity as determined from the pressure field, and a geostrophic wind direction corrected for a veer of  $8^\circ$ . In situations marked by strong cyclonic circulation, the strong veering of the wind between the surface and the geostrophic level (especially along the coast line) will make it virtually impossible to determine the path of a vertical column.

The vertical wind profile is required for the calculation of latent and sensible heat advection through a column wall. The flux advected is the product of the wind component normal to the wall and the particular quantity in question. For the region under study, there are only 2 radiosondes bordering the Gulf whose reported upper winds can be considered representative for surrounding regions. To allow the use of actual upper winds requires a denser network - possibly 5 to 8 stations about the Gulf so as to arrive at a sufficiently accurate wind field. Above 850 mb, where the winds tend to be geostrophic, a height field for the main isobaric levels, constructed from the temperature field, is used to derive the geostrophic wind at these levels. The friction layer, generally extending from the surface to 1000 to 2000 meters above the ground, is a function of the wind, stability, and geostrophic advection of warm or cold air. The accuracy obtained in using a formula such as the Ekman spiral formula, to define the winds in the friction layer, is therefore doubtful. The author therefore assigned a wind equal to 80% of the surface geostrophic wind force for the layer above the laminar layer as previously discussed. The wind force for the intermediate levels in the friction layer, below the geostrophic level, was then linearly

interpolated. In this study, the surface geostrophic wind field was generated from the surface pressure field. This results in the disappearance of both small scale eddy systems as well as orographic effects which influence the surface wind.

Benton and Estoque (1954), and Palmén and Soderman (1968) both utilized geostrophic winds. In their investigation, Palmén and Soderman also used actual upper wind reports. From moisture and energy budget analysis, the merits in using geostrophic winds for the lower levels of the atmosphere can be assessed.

Above the 850 mb level, the mass between any two significant isobaric levels is constant along any polygon about the Gulf Area. Therefore, using geostrophic or actual wind reports in flux advection calculations will not generate fictitious mass convergence. In the layer extending from the 850 mb level to the surface, the fluctuating 850 mb height field results in varying isobaric mass in air columns along any polygon about the Gulf. To prevent fictitious mass convergence, the isobaric mass along the polygon is corrected by the following method:

$$\text{THICOR} = \text{DP} \cdot \text{DPMN}^{-1}$$

where THICOR = correction applied to the term FX (see equation 7),

DP = the isobaric mass of an air column on the polygon boundary,

DPMN = mean isobaric mass between 850 mb and the surface along the polygon.

#### 3.1.4 Accuracy of Interpolated temperature and Moisture Fields

The following section discusses situations where the interpolating scheme will be unable to depict accurately representative vertical profiles of temperature, humidity, and cloud, assuming that the initial data were correct.

Consider a homogeneous air mass moving over three grid points - 1, 2, and later passing over grid point 3, where stations 1 and 3 are radiosondes and 2 is a surface reporting station. If, after passing over station 2, the air mass undergoes extensive modification arising from a warmer underlying

surface, and modification fails to reach the next reporting level, say 850 mbs, the interpolated vertical profile of station 2 will be identical to station 1. If modification however, exceeds 850 mb, the linearly interpolated vertical profile of station 2 will have the largest errors of humidity and temperature at the 850 mb level, the magnitude of the error decreasing as one approaches the ground. Since the cloud field of station 2 is available, it is "exact" and station 3 has no influence on it.

Consider the case where station 2 is a grid point only. In this situation, the surface temperature is interpolated and therefore not exact. Similarly, if modification reaches 850 mb, the total low level profile of humidity and temperature will be erroneous, the extent of the error depending on the spacing of station 2 from stations 1 and 3. Similarly, the entire cloud profile will be an interpolated profile. A clear sky may now become cloud-covered, or visa versa.

Thus, a sparse radiosonde network about a water body requires a denser network of shore based synoptic stations to yield fairly representative profiles of vertical temperature, cloud, and moisture in the horizontal. Over the water regions, however, sharp gradients of temperature and humidity, such as those which occur during arctic outbursts, will not be revealed. It is these sharp discontinuities which are at times critical in energy flux exchanges at the surface.

Figure 3 illustrates the air-sea temperature difference and the corresponding sensible heat exchange occurring during the motion of a dry arctic air parcel over a water body having a surface temperature of  $1^{\circ}\text{C}$ . The flux exchanged was estimated by the program "VERA" (Vowinckel and Orvig, 1972) and the air-sea temperature difference was obtained as a result of a model developed by the author and which vertically redistributes the fluxes exchanged. As seen from diagram 3, the exchange rate at the interface is not constant. Similarly, the air-water temperature difference decreases rapidly at first. The non-linearity of flux exchange is clearly visible. Since the interpolated field cannot reveal such a fine resolution, an attempt was made to redefine the lower temperature and humidity profiles as functions of the stability, water temperature, and the existing flow pattern over the region in question.

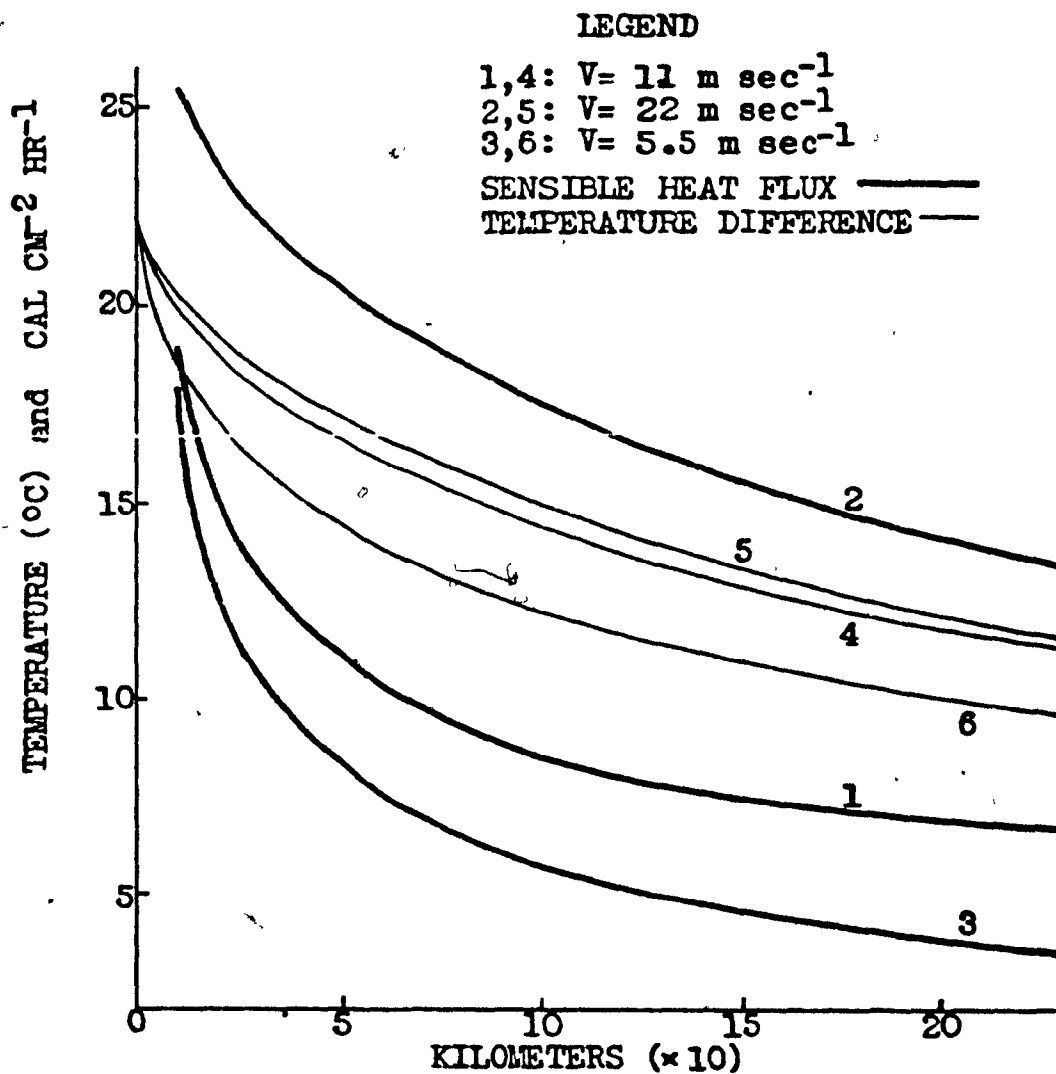


Fig. 3 Sensible heat exchange rates (curves 1,2,3), and air-sea temperature difference (curves 4,5,6) for three different speeds.

For the case of a warm air mass over a colder water body, the underlying surface cools the air, thereby increasing stability in the lower levels. Consequently, the height to which modification reaches is limited, and interpolated temperature, cloud, and humidity fields would approach closely the true state for regions having small gradients of the mentioned parameters. The following section discusses further the need for increased resolution in the temperature and humidity fields when calculating flux exchanges associated with an ice-water body surface.

### 3.2 Latent and Sensible Heat Fluxes

The following sections discuss the flux exchange rates under varying interface situations as calculated by the program "VERA" (Vowinckel and Orvig, 1972), and demonstrate the importance of redefining lower levels of temperature and humidity profiles.

Curves 4 to 6 on figure 3 reveal the rate at which the air-sea temperature difference changes with distance for an atmospheric sounding having temperature and humidity as shown in figure 5 and denoted by ZV. As one would expect, the slower air parcel does attain a higher temperature. Curve 6 shows a 4 deg. C increment after a distance step (10 km), while curve 5 increments by only 2 deg. C. After five distance steps, which is approximately 1/5 of the total distance to be traversed, the air-sea temperature has attained 50% to 80% of its total change for curves 5 and 6, respectively. It clearly demonstrates the required resolution for a desired interpolation scheme to reveal areas of high flux exchange rates. The average resolution attainable over the area under study is much greater than 100 kms.

Diagram 4 indicates the cumulative latent and sensible flux exchanges and flux exchange rates of an air parcel (figure 5) advected with three different speeds over a homogeneous water surface chosen to have a temperature of 1°C. Although curve 3 indicates a large flux exchange due to the longer residence time over the water, the net flux outflow is much lower than that of curve 1 whose velocity is twice as great. For curve 2, whose velocity is  $22 \text{ m s}^{-1}$ , the accumulated flux is almost as great as that in case 1; however, since the velocity is twice as great, the net flux outflow is

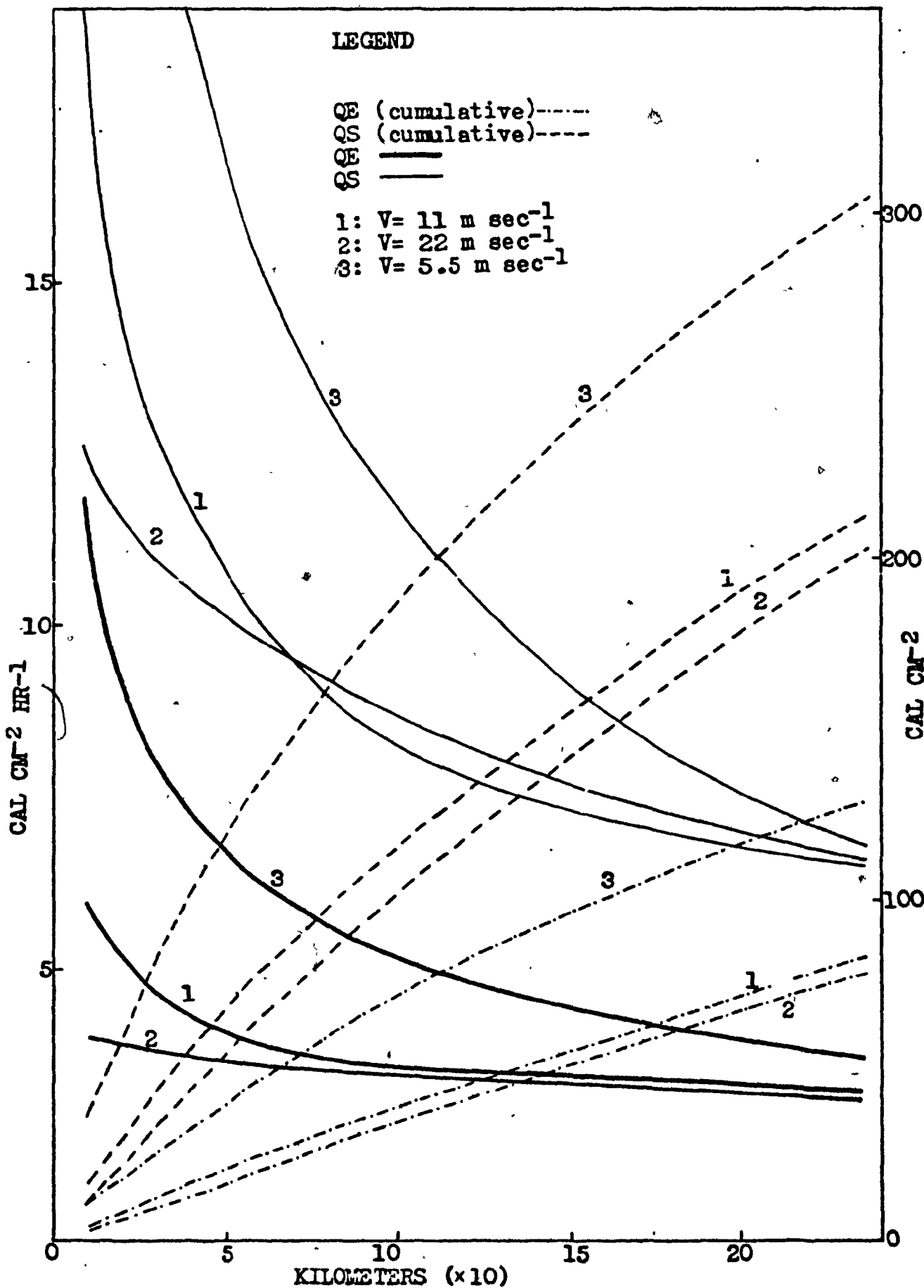


**Fig. 4 Latent and sensible heat fluxes against distance from the departure point.**

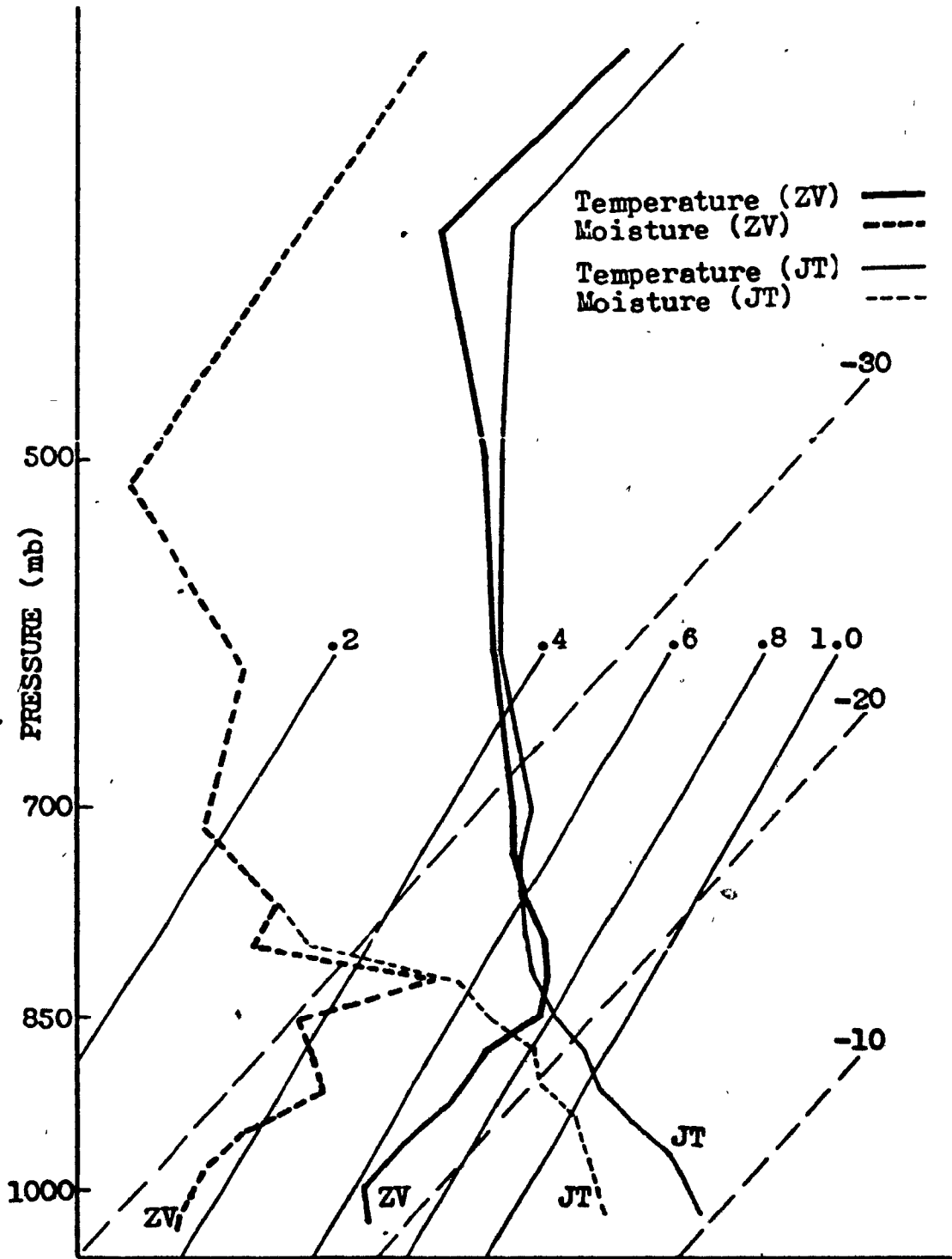


Fig. 5 Temperature ( $^{\circ}\text{C}$ ) and moisture ( $\text{g kg}^{-1}$ ) sounding for Sept Isles (ZV) and Stephenville (JT) for December 16, 1970 at 00Z and 12Z respectively.

approximately twice as large. Figures 6 and 7 illustrate the effect an underlying ice-water surface can have on the rates of latent and sensible heat flux exchanges as computed for an advected profile.

In figure 6, case 1, an air parcel moves with a speed of  $11 \text{ m s}^{-1}$  with various ice amounts along its trajectory - the ice temperature chosen to be  $-10^{\circ}\text{C}$ . As seen between curves 1 and 5, figure 6, an ice surface of  $-10^{\circ}\text{C}$  reduces outgoing fluxes of QE and QS by 50% from a water body having a temperature of  $1^{\circ}\text{C}$ . As indicated by the slopes of curves 1 and 5, the rate of transformation is significantly reduced, thereby indicating that maximum exchanges occur near open ice and/or land-water edges. For total ice cover, latent and sensible heat releases are small (curve 5 of figure 6).

Curves 1 to 5 of diagram 7 reveal the intensity of flux exchanges occurring when an air mass passes from an ice water surface to an all water surface in the last half of its trajectory. Curves 1 and 2 reveal that small ice amounts do not alter the exchange rates appreciably. As ice cover increases, the initially high exchange rates near the leading edge of water, associated with initial outbursts, now occur at the ice-water edge. This sudden increase of QE and QS, accumulated with smaller flux inputs from passage over ice fields, results in rapidly redefined profiles of temperature and humidity a short distance from the leading ice edge.

Physical processes, such as ice formation, are critically dependent on the energy balances at the surface. Linear interpolation of the meteorological terms can lead to errors in the flux exchange pattern. In essence, simple interpolation programs applied to areas like the Gulf, having little internal information, result in a general spreading out and weakening of high flux areas, and regions near leading water or ice edges have little influence on ice formation. This results in larger ice generating areas.

For the region under study, ice formation is restricted to a few areas, while the remaining areas receive most ice through advection by wind and currents.

### 3.3 Behavior of Radiative Terms to Meteorological Parameter Changes

The fact that the turbulent fluxes are highly affected by air mass

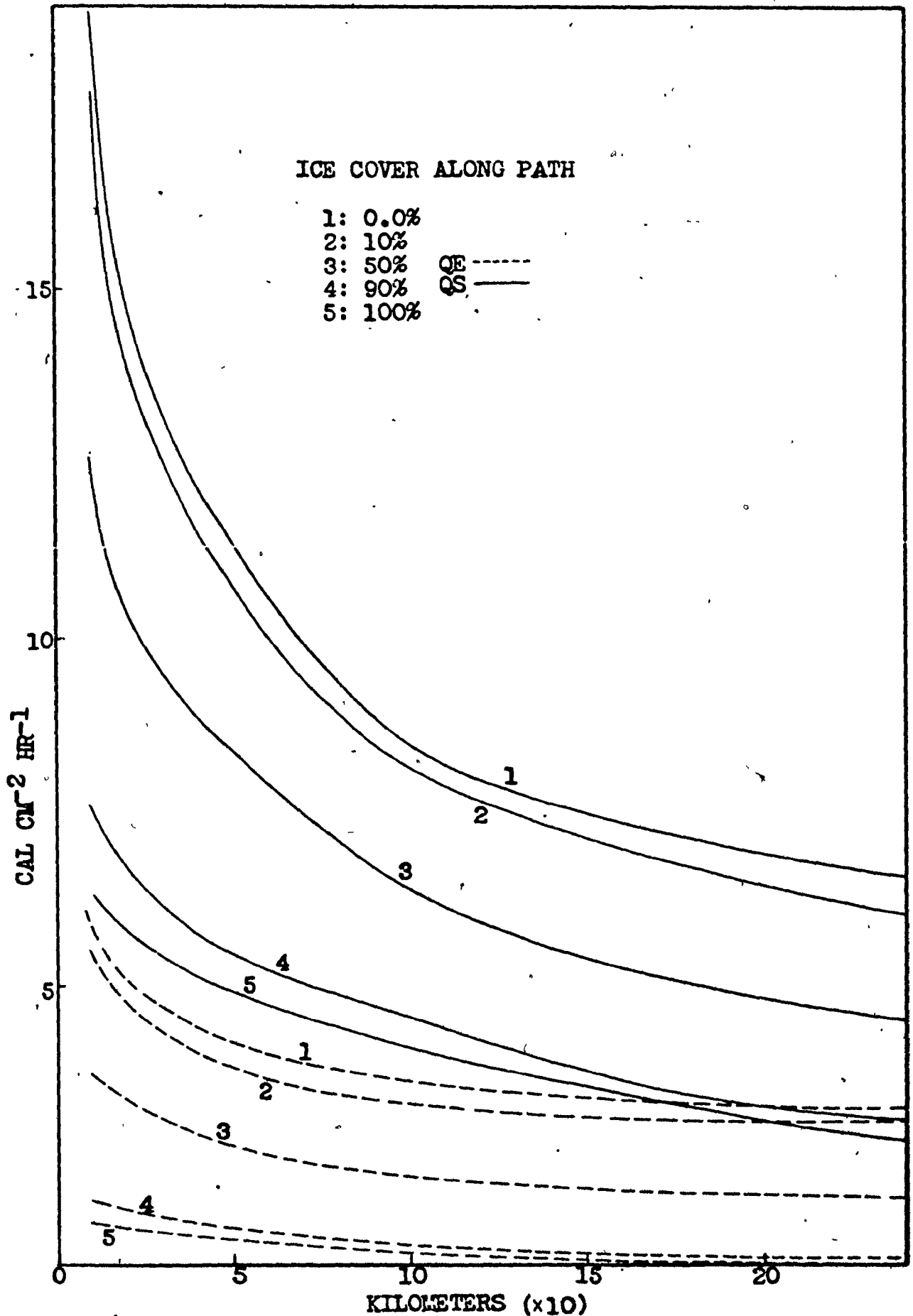


Fig. 6 Latent and sensible heat fluxes against distance from the departure point for various ice areas.

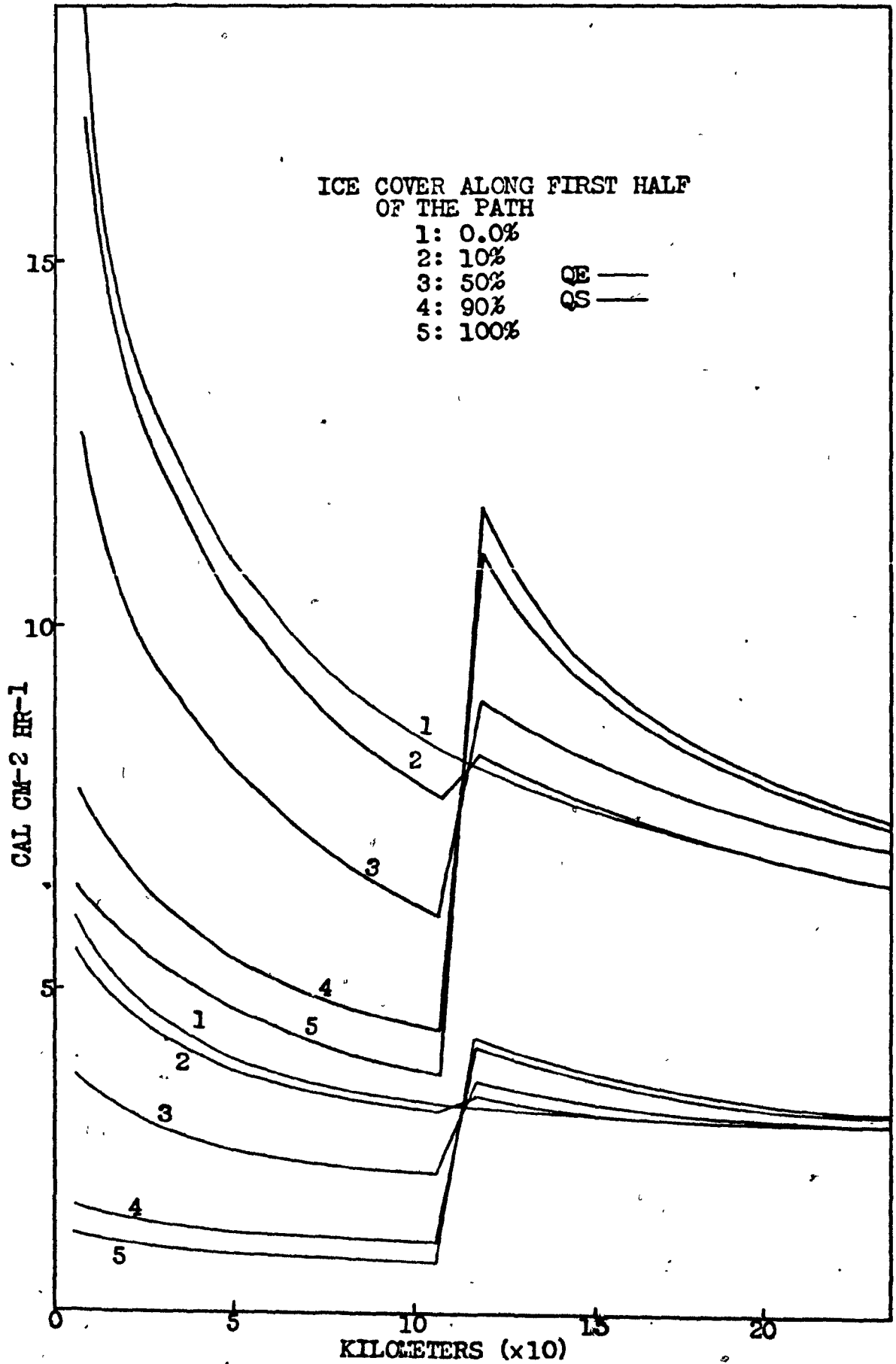


Fig. 7 Latent and sensible heat fluxes against distance from the departure point for various ice areas.

transformation was discussed in the previous section. Calculation of the relevant terms requires transformation of the surface air temperature and moisture fields. The following sections discuss the sensitivity of long and short wave radiative terms, not only with respect to moisture and temperature, but also with respect to cloud amounts, base, and top.

### 3.3.1 Short Wave Radiation

Diagram 5 gives typical vertical humidity and temperature soundings, in particular, Seven Isles (ZV) and Stephenville (JT). Table 2 illustrates changes in long wave downward radiation (DFL) and long wave upward radiation (UFL) - when the vertical temperature sounding is increased by 4 deg. C and the specific humidity doubled or halved throughout. UFL and DFL are in calories per cm<sup>2</sup> per hour.

TABLE 2  
CHANGES IN LONG WAVE RADIATION AS A  
FUNCTION OF TEMPERATURE AND MOISTURE CHANGES

		A	T+4°	2*SH	.5*SH
ZV	UFL	15.5	15.9	15.5	15.5
	DFL	13.7	14.6	14.4	13.2
JT	UFL	15.8	15.9	NA	15.8
	DFL	21.3	22.6		21.1

where T = temperature,

SH = specific humidity,

A = UFL and DFL as derived for ZV (dia 14),

NA = not available as super saturation conditions do not exist.

As seen from table 2, the maximum error in halving or doubling humidity is less than 7%. Similarly, increasing the temperature by 4 deg. C leads to a maximum error of 8%. As such change in humidity is excessive and rarely encountered, the error in large changes would on the average be much less. Similarly diagram 1 illustrates the changes in SAA with varying cloud amount and thickness. The maximum change in SAA amounts to about 25%. Since an estimate of cloud pattern will, in general, never be completely erroneous, the actual discrepancies should, in most cases, be much smaller and limited to times when there is an extensive area of erroneous or missing

data. In relation to the sensible heat exchange (QS), SAA amounts to about 10% to 20%. The next section discusses the effect of clouds on the long wave radiative terms and examines the need for precision in the cloud pattern.

### 3.3.2 Long Wave Radiation

Figure 8 illustrates changes in upward long wave radiation - UFL - and downward long wave radiation - DFL - as cloud amounts are changed, as tops are raised, and as bases are lowered. Two soundings have been chosen. The first is basically a dry sounding with a layer of cirrus. The second is a moist sounding with a deep cloud layer. The sounding at Seven Isles, denoted by ZV in figure 3, has an initial layer of cirrus based at 400 mb and topped at 300 mb. As the cloud cover occupying 10% of the sky is lowered, the down flux, curve  $DFL_1$  in figure 8a, shows little change. Similarly the up flux, curve  $UFL_1$ , shows little change. With only 10% cloud cover, one would expect little change in the radiation pattern. As the cloud amount increases, the downward flux increases. Such an increase is expected, because increasing cloud cover tends to raise the black body flux contribution from this corresponding atmospheric level. From curves  $DFL_1$  and  $DFL_{10}$  of figure 8a, the maximum change in down flux for a given cloud cover lowered 700 mb occurs under overcast conditions -  $DFL_{10}$ , thereby increasing DFL by at most 8%. On the other hand, a change in cloud amount from 1/10 to 10/10, changes DFL from 8% to 20% (curve  $DFL_1$  to  $DFL_{10}$ ) during the same 700 mb range. From this set of DFL curves, knowledge of the cloud amount seems to be most critical. Examination of the UFL curves of figure 8a reveals that, at very high levels, increasing cloud cover from 1/10 to 10/10 decrease UFL by about 20%. One would expect such a large decrease since high level overcast prevents radiation from warmer surfaces of below from escaping through the top of the atmosphere. The maximum change in UFL (20%) for a particular cloud cover with maximum height changes again occurs under overcast conditions. One interesting feature is the convergence of the UFL curves. This is expected as, when cloud levels are lowered, they approach the radiating temperature of the earth. At the lowest level, the black body flux of both cloud and earth surface at a common radiating

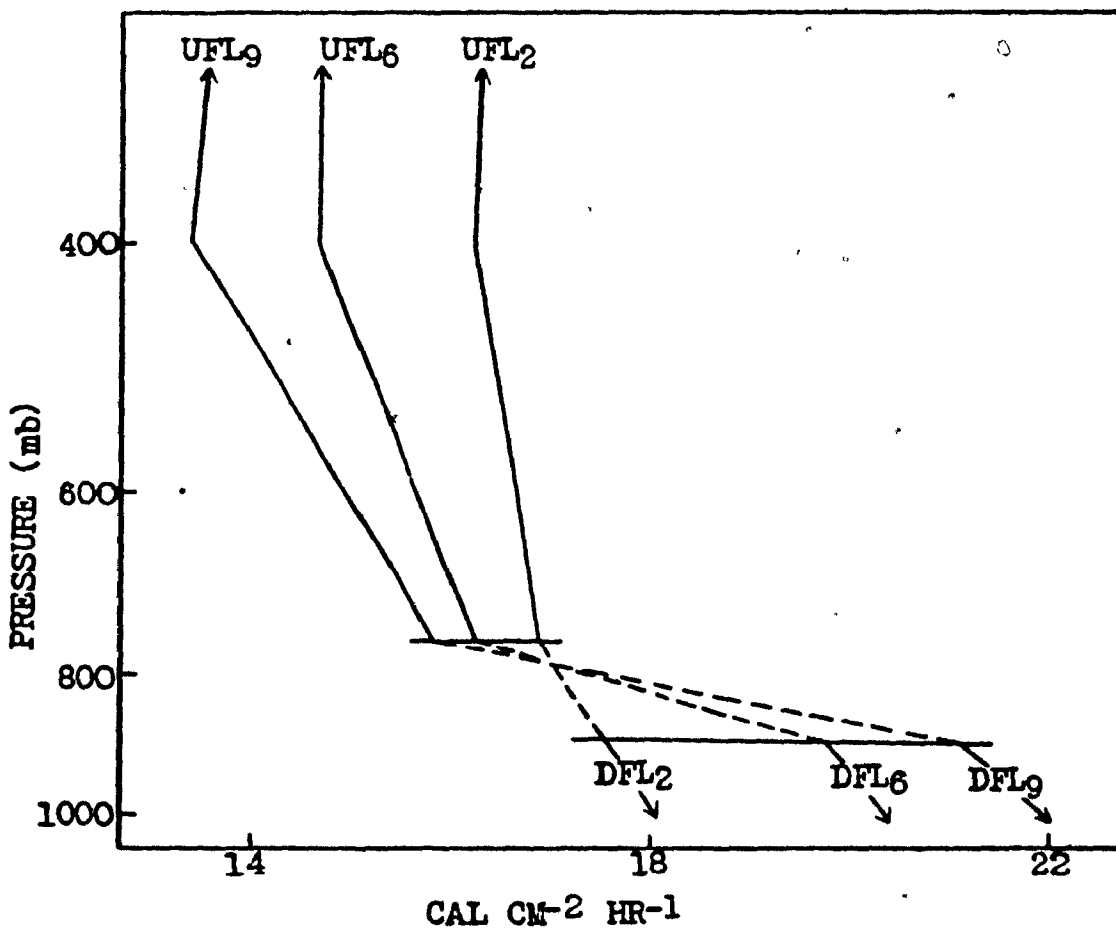
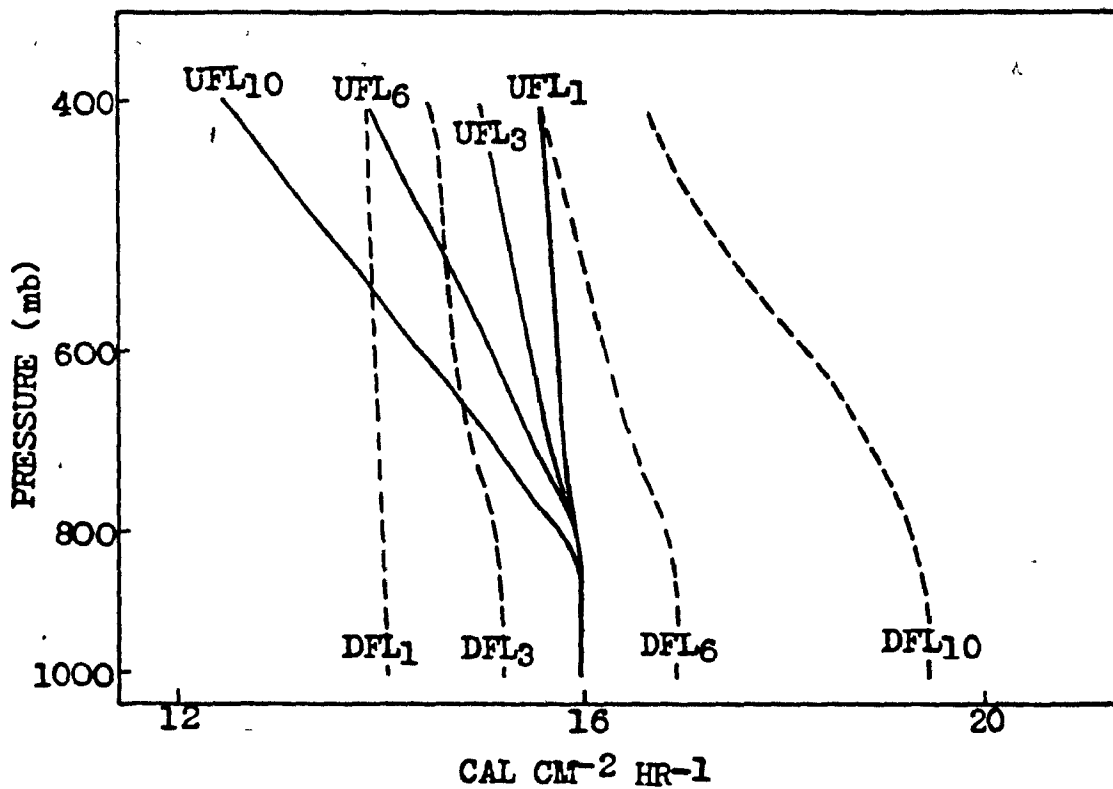


Fig. 8 Long-wave upward and downward radiation emitted by varying cloud amounts at varying heights.

temperature is indistinguishable, thereby indicating that for situations having only low level clouds, accurate knowledge of the correct cloud amount is not essential when calculating UFL.

The sounding at Stephenville, denoted by JT in figure 5, has an initial cloud base and top at 940 mb and 760 mb respectively - see figure 8b. For different cloud amounts, the base has been lowered (arrows downward) and the tops raised (arrows upward). As seen from the DF curves cloud amount changes are more significant than base height changes. In this situation, a change of about 80 mb of the base, changes DFL by about 5% for any particular cloud cover. However, increasing cloud cover from 2/10 to 9/10, increases it by about 20%. From the UFL curves, increasing cloud cover from 2/10 to 9/10 decreases UFL up to a maximum 20%. This is comparable to the figure derived in diagram 8a, where cloud amount is increased from 10% to 100% of the sky area (curves  $UFL_1$  and  $UFL_{10}$ ). Similarly, the maximum change of UFL associated with a particular amount of cloud with maximum height changes occurs under overcast conditions -  $UFL_{10}$ . From these two diverse vertical soundings, it appears that cloud amount is the critical factor for DFL, and equally cloud amount and height for UFL.

This section reveals the non-linearity of the radiative terms, resulting from modification of the temperature, humidity, and cloud profiles of a vertical sounding advected under various conditions over various interfaces. The QE and QS curves 1 to 3 of figure 4 <sup>are</sup> is the cumulative flux exchange for an air parcel advected for 3 different speeds over a water body. The DFL curves 1 to 3 of figure 9a is the corresponding downward long wave radiation. As to be expected, the slower moving parcel receives the greatest amount of flux contributions by the underlying surface per unit distance travelled. Similarly, the non-linear increase in DFL after the first few distance steps, curve 3, again reveals the non-linearity of the radiative terms associated with cloud formation. Curves 1 and 2, with lesser modification, show similar non-linear increases in DFL. The area enclosed between curve 1 of figure 9a and the dashed line is the difference between DFL along the trajectory and DFL as obtained by a linear interpolation of the cloud, temperature, and humidity profiles of the initial and final sounding. The maximum underestimate associated with the linear

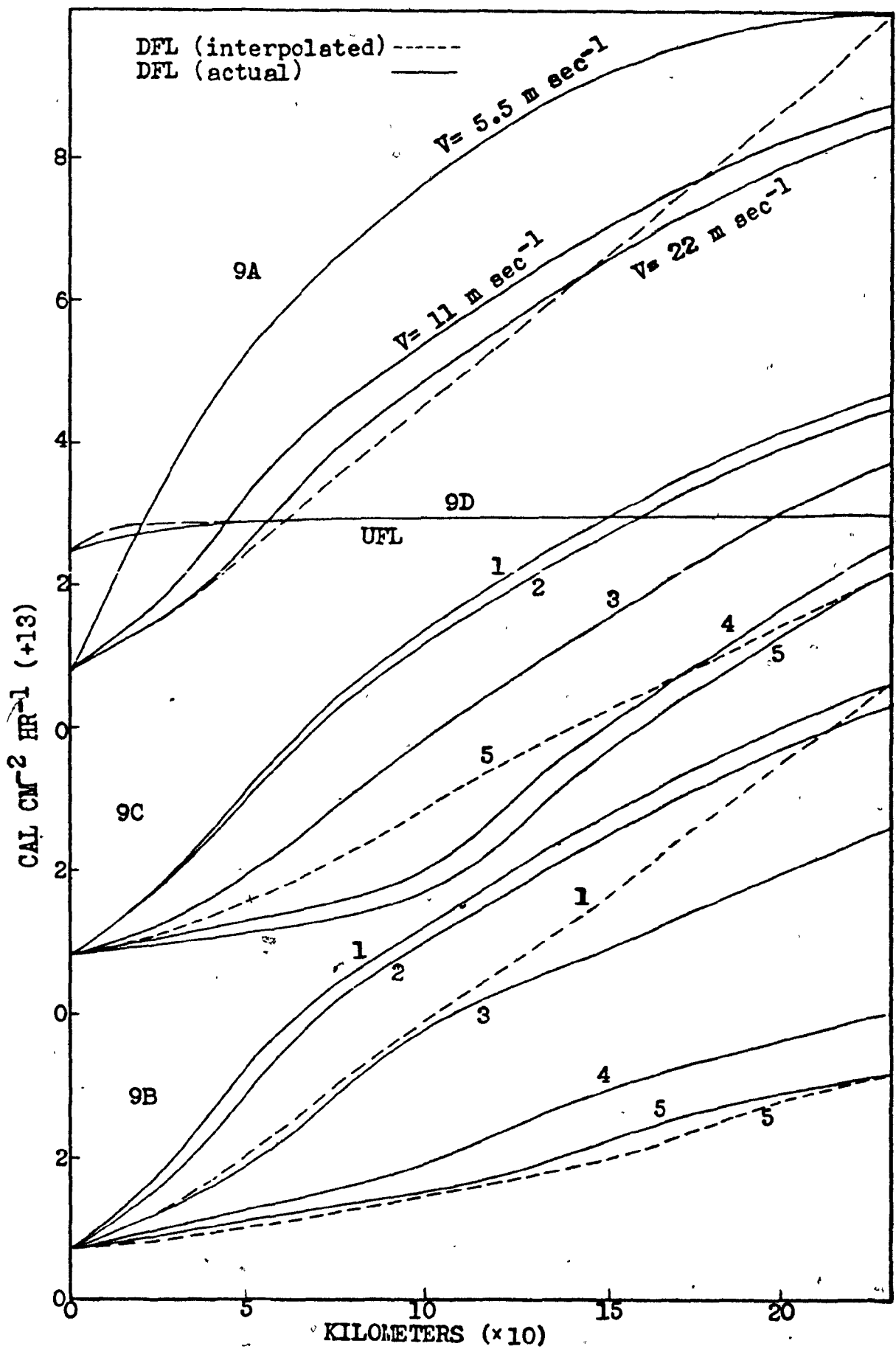


Fig. 9 Long-wave radiation upward and downward against distance from the departure point.

interpolation is 12%. Underestimates of UFL are negligible as shown by the UFL curves of figure 9d.

Figure 6 examines the flux exchange rate and pattern for a profile advected over a water surface with constant ice areas along its path. The corresponding curves of DFL are shown in 9c. They reveal an initial sharp linear increase in DFL as the air becomes transformed, followed by a non-linear increase. The slow exchange rate depicted in curves 4 and 5 of figure 6 for the case involving almost total ice cover, results in an almost linear increase in DFL - curves 4 and 5 of figure 9c up to the ninth distance step, after which cloud formation increases DFL non-linearly. The area enclosed by the dashed and solid lines of curves 1, 3 and 5 indicate the difference between the down flux DFL along the path of advection and the down flux associated with intermediate interpolation of the initial and final temperature, humidity and cloud profiles. As modification decreases, the error becomes negligible as in curve 5 of figure 9c.

Figure 9b illustrates the down flux (DFL) of a profile advected with ice areas along the first half of the path, and all water surfaces in the last half. Curves 1 to 5 of diagram 9b clearly show the effect of an ice cover on cloud formation and the radiation pattern. In curve 1, figure 9b, the first two steps show a linear increase in DFL followed by a sharp non-linear increase in DFL due to cloud formation at about the third distance step. In curve 5, the slow exchange rates over the total ice-covered region for the first half results in an almost linear increase in DFL. After the 11th step, passage over warm water results in quick cloud formation, accounting for the rapid non-linear increase in DFL. Again, the non-linearity of the radiative terms, with respect to meteorological parameter changes, namely cloud structure, is revealed by curves 4 and 5 of diagram 9b. The enclosed areas of diagram 9b denote the difference between actual computed values of DFL and those values derived by interpolating intermediate profiles of the required parameters using only the initial and final profile. Examination of diagram 9b reveals one very interesting feature. While linear interpolation underestimates the downward flux in diagrams 9a and 9c, one will notice that in the case of curve 5, figure 9b, linear interpolation overestimates the downward flux in the region over the ice-water edge. With

respect to surface budget analysis, this overestimate would erroneously retard ice formation at the leading ice edge. Figure 9d indicates the upward radiation flux (UFL) lost to space. Since most changes are located in the lower levels, UFL (solid line) showed little difference in all situations examined. The dashed line was the linear interpolated flux profile and as can be seen, the difference is insignificant.

### 3.3.3 Heating Rate

The heating rate of the atmosphere attributable to the long and short wave radiation is given by

$$\frac{\partial Q}{\partial T} = RLU - UFL - DFL + SAA$$

For all the various cases outlined by diagram 8a and 8b, the long wave contribution from the atmosphere to the heating rate varies by 20%. This indicates that excessive errors in reported cloud amounts and heights are required for significant heating rate errors. On the other hand, the surface budget has, as one of its terms, DFL. During critical periods, such as ice formation which is the result of energy imbalances, erroneous values of DFL could be crucial. Lettau and Davidson (1957) have shown that under clear sky conditions, 90% of the back radiation comes from the lowest 800 m to 1600 m of the atmosphere. It is therefore important that representative vertical soundings be obtained for cloud, temperature, and humidity in the lower levels.

From the examination of the behavior of radiation terms, it becomes evident that the effect of radiative heating during step-wise calculation of air mass modification can be neglected. On the other hand, air mass modification schemes must consider not only changes in sensible and latent heat due to exchanges at the interface, but also changes in the cloud pattern so that an adjusted cloud field may be generated and the down flux, an important component of the surface energy budget, may be reasonably estimated.

### 3.4 Nephanalysis

The cloud analysis for the area under study is based on the following

available data: low cloud amount, type and height, middle and high cloud type, total amount of cloud, and the present weather as denoted by symbols  $N_H$ ,  $C_L$ ,  $H$ ,  $C_m$ ,  $C_H$ ,  $N_T$ ,  $ww$ , respectively. Under international standards, each symbol is represented by a number, usually from 1 to 9. In the case of  $ww$ , numbers 0 to 99 describe various weather situations occurring at the reporting time. During periods of inclement weather, when visibility is poor, information about mid and upper levels is impossible to obtain. Similarly, transmission errors may result in some erroneous reports. To make the most effective use of the reported cloud data, the author examined five locations - Grindstone, Fox River, Seven Islands, Charlottetown, and St. Andrews - (General Summaries of Hourly Weather Observation - Nov. 52 to Feb. 53) to determine the predominant cloud height and type over the surrounding Gulf regions. Stratocumulus occurred for more than 50% of the time at all these points. Next was stratus and stratus fractus. The most frequent heights reported were roughly between 1600 and 3600 feet. Before interpolation of the cloud field in the horizontal and vertical proceeds, the cloud data are checked as described below.

If any of the following elements were missing -  $N_H$ ,  $C_L$ ,  $C_m$ ,  $C_H$ ,  $H$  - the term  $ww$  was used to help fill in the gap wherever possible, using the subroutine ZNEPHE. For weather situations characterized by fog or fog banks, the cloud amount (ACD) is usually coded as obscured. If the weather type reported was fog, the bottom layer was assumed overcast with above levels recorded as missing. If significant precipitation was reported, the five bottom layers were assumed overcast. If the cloud height ( $H$ ) for reported low cloud is missing during fog - like situations,  $H$  was assumed to have a value of about 100 feet. If the reported cloud type ( $CL$ ) was stratus or stratus fractus,  $H$  was assigned a value of 1600 feet. In all other cases, the height assumed for reported low cloud and missing height reports was about 2500 feet. For cases of missing low cloud type and  $ww$  greater than 90 - that is, moderate to severe weather - the cloud type assumed was heavy cumulus. Analysis of four months revealed only 2 hours of reported cumulonimbus. This low figure may be due to the fact that cumulonimbus activity is embedded in obscuring cloud fields. However, due to the Gulf waters being rather cold ( $-1^{\circ}\text{C}$  to  $2^{\circ}\text{C}$ ), heavy cumulus

development would occur during only the coldest arctic outbursts as compared to frequent development over the Japan and China Sea where sea temperatures range up to  $8^{\circ}\text{C}$  and  $20^{\circ}\text{C}$  respectively.

If low cloud amount ALC is missing and fog and drizzle like conditions were reported, low cloud amount was taken to be 9/10 of total reported cloud amount ACD. Under these situations, low cloud amounts usually accounts for almost all the reported cloud. If the weather reported was associated with light to heavy precipitation and where the overcast layer often lies from mid to upper levels, the amount of low cloud was taken to be 7/10 of total reported cloud ACD. Otherwise, under fair weather conditions, low cloud was taken to be 4/10 of reported total cloud amount. The justification for using the above described procedures lies in the fact that omitting all station reports having a missing element would have been sufficient to produce a more erroneous cloud field than that obtained by using the above substitutions.

There are instances when a missing element is crucial and no amount of estimating yields a justifiable answer. The following is such an example. If reported total cloud amount (ACD) is missing, and low cloud amount is less than 10/10ths, lack of knowledge of middle and high cloud amount makes it impossible to estimate ACD.

Once the various pieces of information concerning cloud height, type, and amount, have been obtained, the vertical extent of low, middle, and high clouds are determined by a cloud analysis program (Vowinckel and Orvig, 1972). After the cloud amount has been established for 16 atmospheric layers at each valid reporting station, a numerical analysis "INTER" is used to derive a continuous horizontal cloud field at all levels. Next, the lowest reporting cloud level for each grid point is recorded in ICLDHT to be used later in association with cloud formation. The author also examined 60 reports of reported cloud and vertical temperature and moisture profiles (Dec. 1969, Jan. 1970) for Sept Isles and Stephenville to determine the relationship between reported cloud amount and the relative humidity recorded at the reported cloud level. From figure 10, the cloud amount is usually small and negligible when the relative humidity drops below 60%. On the other hand, cloud amount seems to increase significantly when the relative

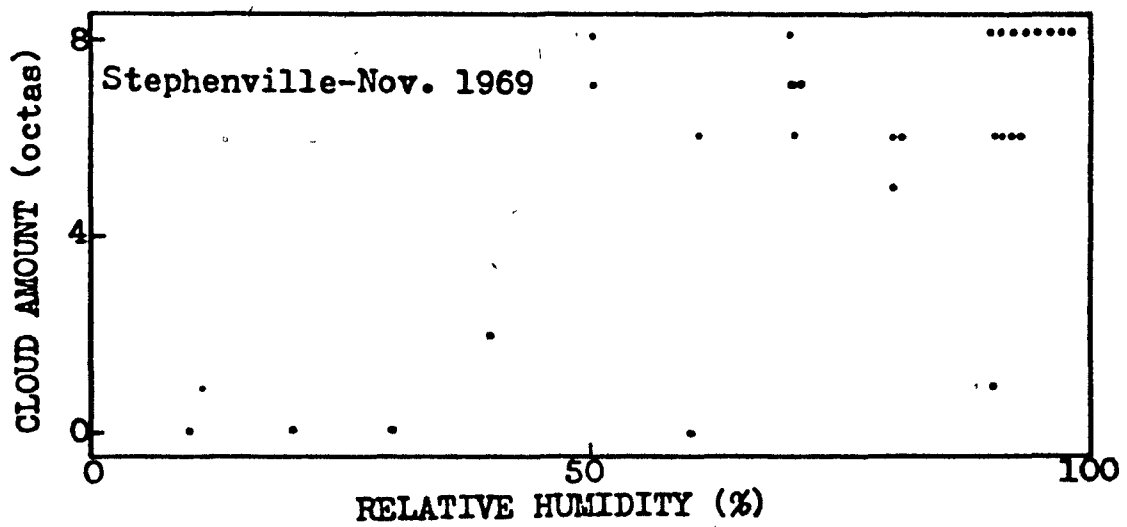
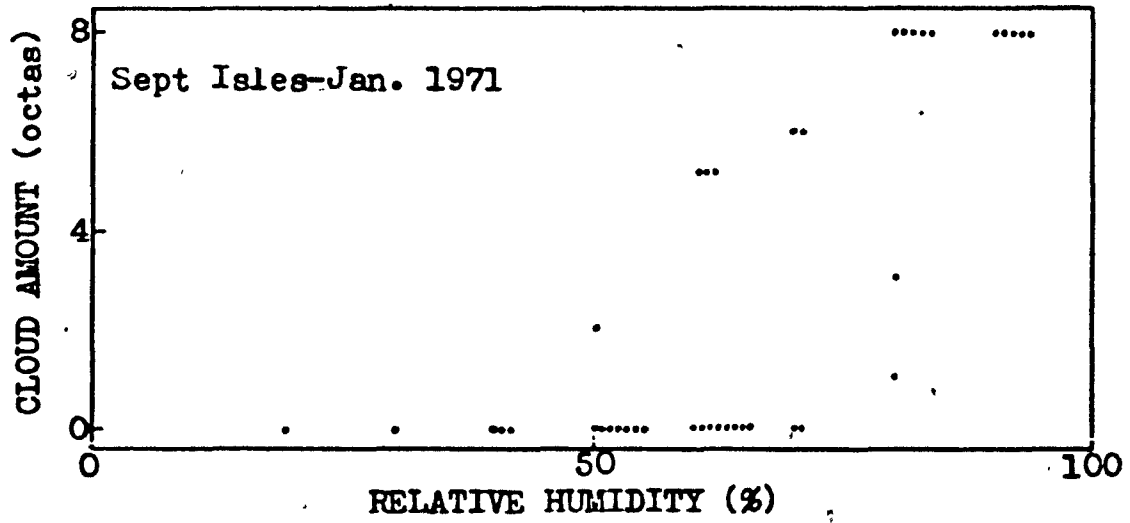


Fig. 10 Cloud amount plotted against relative humidity.

humidity exceeds the 60 to 80% range.

As previously discussed, a good estimate of the low level cloud amount is desirable in obtaining an estimate of downward long wave radiation. Similarly, the surface temperature and humidity were seen to be an important factor in determining the flux exchange rate, the flux distribution, and the long wave flux. The following section discusses a method employed for achieving a better approximation of the lower level profiles of the meteorological parameters essential in evaluating energy budgets, all the while using the initially interpolated fields as a first approximation.

### 3.5 Air Mass Transformation - Model

For the calculation of freeze-up and ice formation over a given area, a detailed knowledge of the energy budget terms is required. Considering foregoing processes, it is doubtful whether simple interpolation programs as discussed so far would result in sufficiently accurate meteorological fields.

Burke (1945) devised methods of predicting the final surface air temperature by using the following parameters: initial air temperature and humidity, sea surface temperature, lapse rate, and distance travelled over water. As a second approximation for required data fields, an air mass transformation program "AIRMTR" was devised by the present author. The underlying principal is an extension of the "Burke" technique applied over a large area.

#### 3.5.1 Advection of Air Parcels

The model used by the author is an extension of one developed by Vowinckel (personal communication). This model calculates intermediate temperature, cloud, and humidity profiles along a streamline - all the while taking into account the varying sea surface temperature, winds, and sea level pressure. This redefined field is then assumed to be in steady state for the next 12 hours during which energy budget computations are executed.

To effect the transformation of certain meteorological parameters in the lower levels, all boundary and ice or water grid points of figure 2

have been specially identified. Next, all points along the Gulf shore are examined to determine if the advection of their profile by the geostrophic wind (veered  $8^{\circ}$ ) is towards land or ice/water surfaces. Profiles overlying regions with off shore winds will then be advected by the subroutine "TRAJEC". This subroutine calculates displacement from one grid line between two grid points to another grid line between two different grid points. The maximum allowable displacement is  $1.44 * DX$  where  $DX$  is the grid spacing. From one grid line to another, flux exchanges at the interface are calculated and redistributed in the vertical, and the modified portion of the profile is recorded at two nearby points. Following this, the entire profile is advected. The grid spacing was chosen as 37 km, so as to include significant bays and straits.

### 3.5.2 Sensible Heat Distribution

Each advected profile has its meteorological parameter changes executed in the subroutine "TEPHI" which simulates the temperature and humidity soundings on a tephigram.

The sensible heat exchange for ice and water surfaces is calculated in the subroutine "HEMLOK" and the subroutine "SCFLEX" appropriately weights the flux contribution from ice and water surfaces. "HEMLOK" is an extension of the subroutine "VERA" (Vowinckel and Orvig, 1972). Following this, the subroutine "EATDST" distributes the sensible heat into the sounding. The level of modification is limited by the maximum lapse rate allowable, and by the magnitude of the sensible heat exchange. Each time the lapse rate is exceeded, another layer is included in the modification process. Examination of several profiles traversing the Gulf and passing over Stephenville showed a lapse rate usually near the midway of the moist and dry adiabat.

In situations of cooling by an underlying surface, the depth of cooling is greatly dependent on the stability of the profile and wind shear. Sellers (1965) summarizes various studies on stability. In general, strong stability is usually characterized by a Richardson number of .25, and -.7 for the unstable situation. The subroutine "RICRDN" determined if an advected profile would develop a low level surface inversion or a cooled layer with a dry adiabatic lapse rate. For a Richardson number greater

than  $-0.2$ , a surface inversion not exceeding 1 layer (about 25 mbs) was allowed to occur, otherwise cooling was extended to include the two bottom layers (about 50 mbs). Linearly interpolated low level winds, the temperature profile, and the height field were involved in the calculation of the Richardson number.

The model was designed to simulate changes in the lower atmosphere which are predominantly effected by underlying surface features and which, in turn, almost wholly affect the energy budget of the underlying surface. Therefore; changes occurring in the higher levels due to warm or cold air advection and large scale vertical motion will not be possible. To include such processes would require advection of an atmosphere divided into several layers, with each layer consisting of a similar grid point array and each layer moving independently of the others with exchanges of moisture and heat occurring between grid points of each layer.

### 3.5.3 Latent Heat Distribution

With respect to moisture, the latent heat is equally added to all modified layers by the subroutine "HUMDST". Following this, the vertical moisture profile is analysed in the cloud formation program called "CLOUD". Each layer is checked to see if the relative humidity exceeds 70%, after which cloud formation is allowed to proceed if the interpolated cloud field indicates that cloud does exist for that particular layer at that grid point. Once overcast conditions are achieved, the maximum relative humidity allowed is 85%. Ninomiya (1964) shows that clouds with a water content of  $.43 \text{ g kg}^{-1}$  had a relative humidity exceeding 85%. Since the Gulf area is not marked by extensive modification as is the air over the Japan Sea, the author chose an upper limit of 85%. After overcast conditions are attained, and after the relative humidity reaches 85%, the excess moisture is transported to the next upper level where it is used to increase cloud and/or humidity. The clouds are assumed to have a liquid water content of  $.2 \text{ g kg}^{-1}$  (Squires, 1958). The highest mean value obtainable is  $.3 \text{ g kg}^{-1}$  under states of very strong convective activity (Warner, 1955).

#### 3.5.4 Islands

Islands such as Anticosti and Prince Edward act as sinks for sensible and latent heat acquired by air masses having passed over ice/water surfaces. These two islands as well as the Magdalen Shallows and the northern portion of Cape Breton Island were treated as solid ice surfaces having a defined temperature - the temperature being that of the nearest reporting station as no ground temperatures are available. During the winter season, the recorded air temperature will generally approximate the surface temperature. For regions lying on the windward shores, the temperature will be largely modified and not representative.

#### 3.5.5 Interface Temperature

One parameter essential in calculating the flux exchange at the interface is the ice/water surface temperature. As previously stated, air parcels are advected from one grid line to another. In the case where the initial and final grid points are water, the water temperature for the first half of the step displacement is the linearly interpolated temperature of the 2 grid points bounding the grid line. Similarly, the temperature of the last half of the displacement is the linearly interpolated temperature of the 2 last grid points involved. In the case of all ice cover, ice temperatures are substituted. For a mixture of ice and water surfaces, the flux contributions from ice and water are calculated and then weighed according to the areal extent of ice or water. The temperatures in these situations are areally weighed.

#### 3.6 Water Body Model

In periods prior to ice formation over the Gulf, the high flux exchange rates associated with cold Arctic outbursts will gradually reduce the finite heat supply of the Gulf. This resulting heat loss, reflected by a drop in the surface water temperature, is a principal factor in determining the flux exchange rate. An accurate estimate of the flux exchange demands a reasonable estimate of the air-sea temperature difference. Preceding sections dealt with the unrepresentativeness of certain meteorological fields in the lower atmospheric levels as generated by simple

interpolation techniques applied to meteorological data. In this section a method is described, which regenerates the parameters essential in evaluating the latent and sensible heat flux exchanges between the atmosphere and the underlying water body. Used in conjunction with a water body model (see Appendix) developed by Lally (1973), and initialized at a date for which there exist scattered vertical soundings of temperature and salinity for the Gulf, surface water temperature distributions are obtained from time step to time step through energy budget considerations and iterative energy balance schemes incorporating modified and unmodified atmospheric and water parameters.

Chapter IV sec. 1.1 examines the limitations of the air model by examining an actual sounding advected over the Gulf with a sounding recorded twelve hours later, and section 4.1.2 discusses the results of applying the advection scheme over the entire Gulf region whose ice/water temperatures are regulated by a water-body model.

## CHAPTER IV

## APPLICATION OF THE MODEL

The preceding chapter discussed the inadequacies of interpolated data fields in revealing high temperature and humidity gradients associated with rapid air modification during arctic air outbursts over the Gulf. The principal component of the air model is the advection, and redefining the profile of certain meteorological parameters with the aim of approximating better the location and magnitude of horizontal gradients of temperature, humidity, and cloud. The parameters of particular interest are the derived surface and air temperatures which are critical factors determining the flux exchange rates at the interface. Similarly, since the downward long wave radiation flux is greatly dependent on conditions in the first 1000 to 2000 meters (see sec. 3.2.2.2), obtaining good approximations of temperature, humidity, and cloud is desirable.

#### 4.1 Advection of an Air Column

Figure 11 illustrates an example of an actual "initial" profile (identified by 0) and an actual "final" profile, identified by heavy line, as well as intermediate profiles produced by the subroutine "TEPHI" for an air parcel moving over a water body along a path shown in figure 13a. The profile, identified by "M", is the moisture profile of figure 12, identified by "0". The product of the profile number and 10 represents the distance in kilometers between the profile and its departure point. The final computed profile is denoted by #23. Curves 1 of figure 4 correspond to its latent and sensible heat input as computed by the model for the profile advected at  $11 \text{ m sec}^{-1}$ . The area, enclosed by "23", and the reported profile (heavy line) is the difference between the computed and the actual profile reported 12 hours later at Stephenville. The character "t" denotes the height of the modification as produced by the model. For reasons discussed in sec. 3.5.2, only the region below the last modified level (denoted by "t") is compared to the actual sounding, in determining the

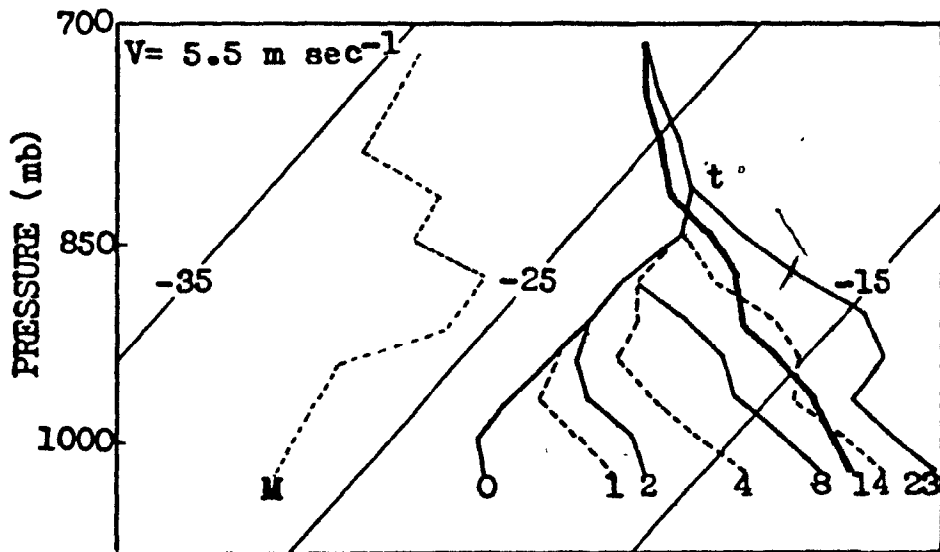
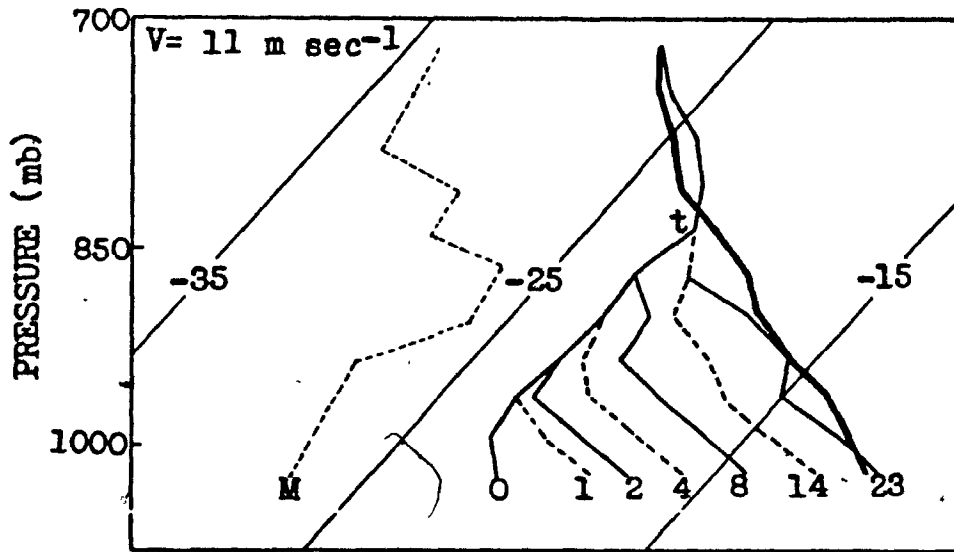


Fig. 11 Tephigram temperature profile ( $^{\circ}\text{C}$ ) of an advected air parcel at various points along the path.

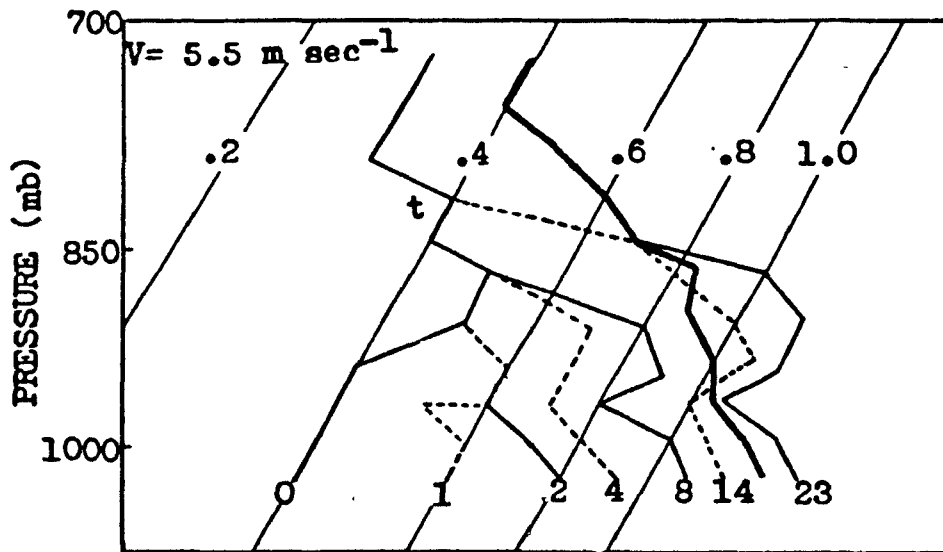
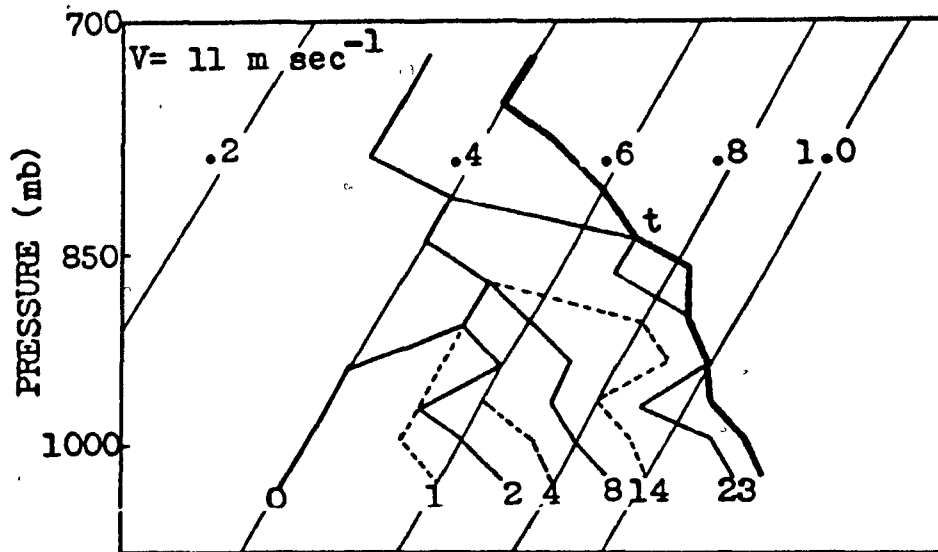


Fig. 12 Tephigram moisture profile ( $\text{g kg}^{-1}$ ) for an advected air parcel at various points along the path.

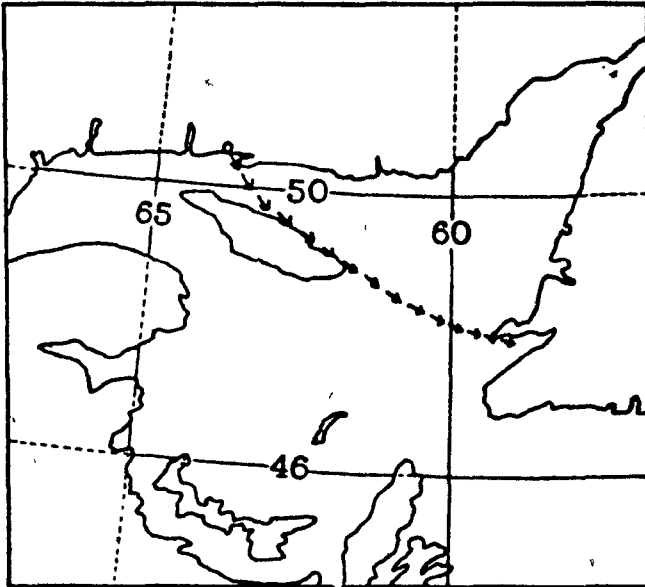


Fig. 13a Path of advected parcel.

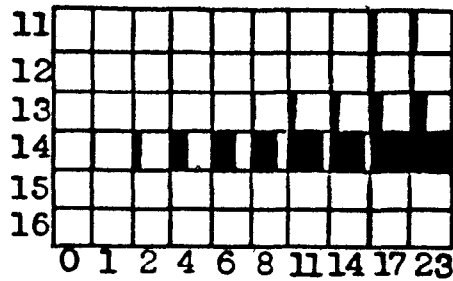


Fig. 13b Cloud thickness and amounts for various points along the path ( $V = 5.5 \text{ m sec}^{-1}$ ).

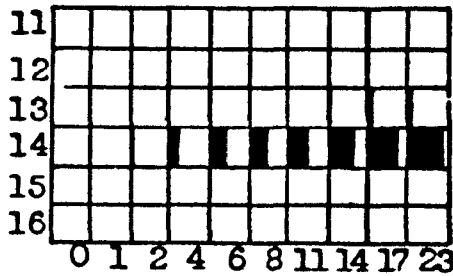


Fig. 13c Cloud thickness and amounts for various points along the path ( $V = 11 \text{ m sec}^{-1}$ ).

effectiveness of the model. In figures 11 and 12, the model accounts for 94% and 90% of the change in temperature and humidity respectively, for a profile advected at the reported speed of  $11 \text{ m sec}^{-1}$ . With respect to the surface temperature and moisture changes, the model accounts for more than 95%. The initial profile was further tested to display the extent of modification which would occur if the velocity was reduced by 50%. In this case, the model overestimates the temperature and humidity change by about 20% and 25%, respectively. The surface temperature and moisture are overestimated by 25% and 8%, respectively.

Figures 13b and 13c show the cloud content in each layer, corresponding to intermediate temperature and moisture profiles of figures 11 and 12. The top of the eleventh layer is 850 mbs, and the base of the sixteenth layer lies at the surface. Each layer is roughly 28 mbs thick, and a darkened square represents total overcast. Verification of cloud extent in the vertical is virtually impossible and orographic effects along the shores will further reduce the reliability of low level cloud reports for near-shore stations. For the sounding advected at the correct velocity, the cloud amount in the lowest layer is slightly less than overcast with greater than 1/10 the cloud cover in the layer above -- each layer being about 25 to 30 mbs thick. The high vertical extent of cloud for the case of the slowly advected profile seems unlikely as only light snow showers were reported at Stephenville.

In choosing profiles, the following conditions were satisfied. The wind direction was not allowed to change by more than  $20^\circ$  from the surface to 850 mb, the wind shear was small, the airmass in the source region was homogeneous for at least 18 hours, and the streamline flow, determined by using the 850 mb contour and wind field for two time periods (12 hours apart), passed over Stephenville. The mean surface water temperature was obtained from sea surface temperature charts.

Due to the interaction of various meteorological parameters in the flux exchange equations, it is virtually impossible to attribute the discrepancy between the model profile and the actual profile to any one parameter alone. In applying the advective scheme to the total Gulf area, the accuracy will vary of basic meteorological parameters involved in the flux exchange equation.

The derived wind field, water and air temperature, humidity, and the exchange coefficients are the factors having the greatest influence on the flux exchanges. In the model, the accuracy of the geostrophic wind is limited by the accuracy of the reported pressure data, whose errors can be considered negligible when transmission errors are absent. The wind field, derived from the pressure gradient, may produce spurious high winds as the pressure gradient pattern will not be exactly duplicated. Over a sufficiently long time period, spurious high gradients will have negligible effects on the cumulative energy and moisture flux exchange. During ice formation periods the presence of ice, as determined by the water body model, may be erroneously present. Because the ice temperature approaches the air temperature, these grid points may depart actual on site temperature by 5 to 10 degrees. Above the surface, the estimated temperatures and humidities will be significantly more accurate. In both instances, the estimated value will reduce considerably the errors obtained in using mean climatological or strictly interpolated fields derived from surrounding Gulf stations. Because of the length of time involved, as well as the number of grid points, the significance of these spurious errors will be reduced considerably. The greatest uncertainty lies with the exchange coefficients which depend on both wind and the vertical gradients of temperature and humidity. Since these coefficients are empirically derived from observations over long time periods with varying synoptic situations, such as encountered in this study, the flux exchanges will tend to be accurate in the mean and during periods of significant flux exchanges.

The following section examines air mass transformation over the entire Gulf area and the resulting changes in the surface temperature and humidity fields, as produced by the model.

#### 4.2 Air Mass Transformation over the Gulf Region

The previous section discussed the advection of a single profile. Subroutine "AIRMTR" was designed to record the cumulative effects of numerous advectations over ice-water surfaces with varying temperatures, namely the temperatures derived from a water body model (see Appendix). Anticyclonic situations were examined to determine if off shore temperature

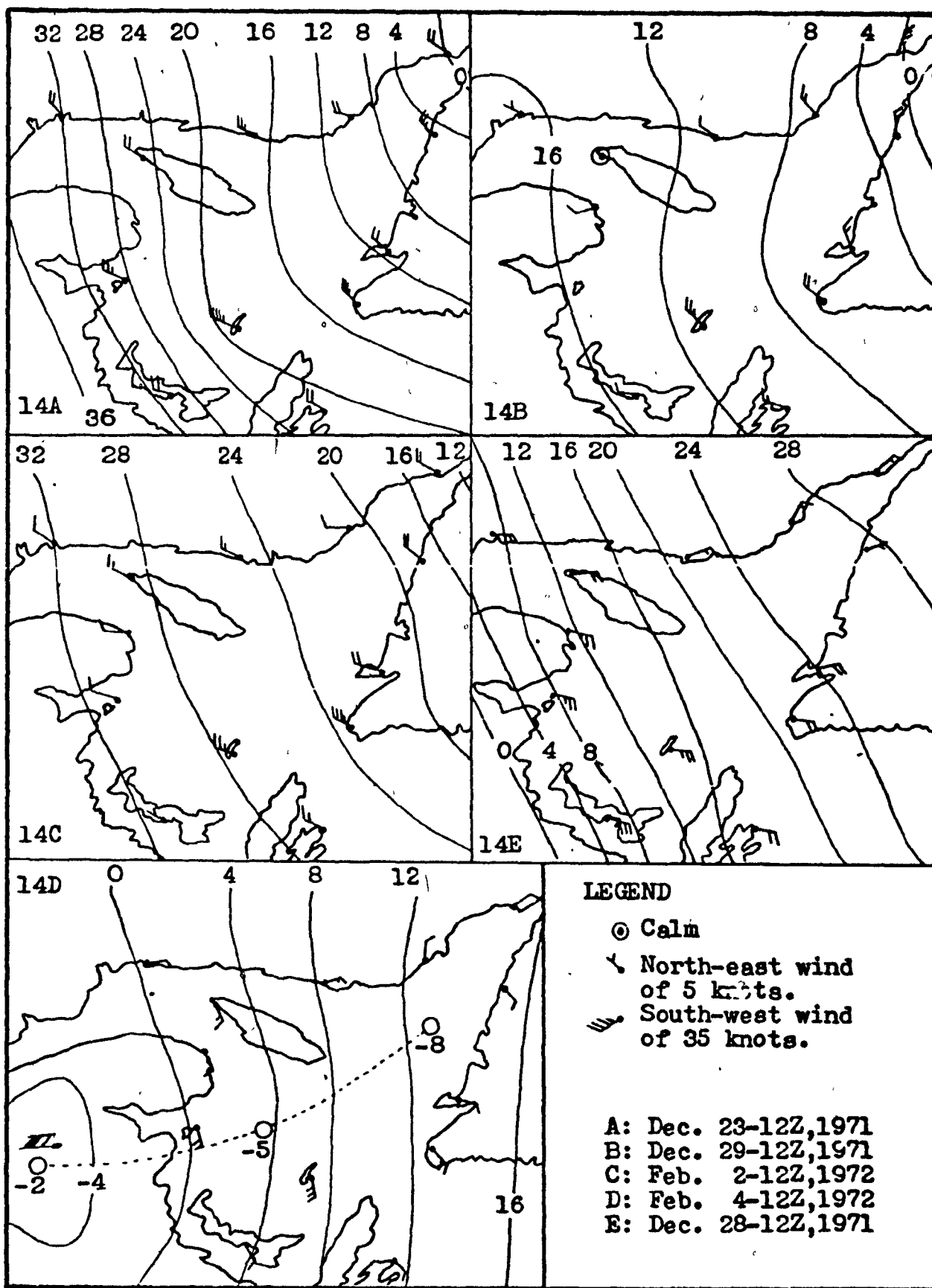


Fig. 14 Mean sea-level pressure (mb.+ 1000.) and reported winds for five synoptic situations.

Fig. 15 Transformed temperature field (—°C)  
and changes (---°C) from the initial  
field for Dec. 29, 1971.

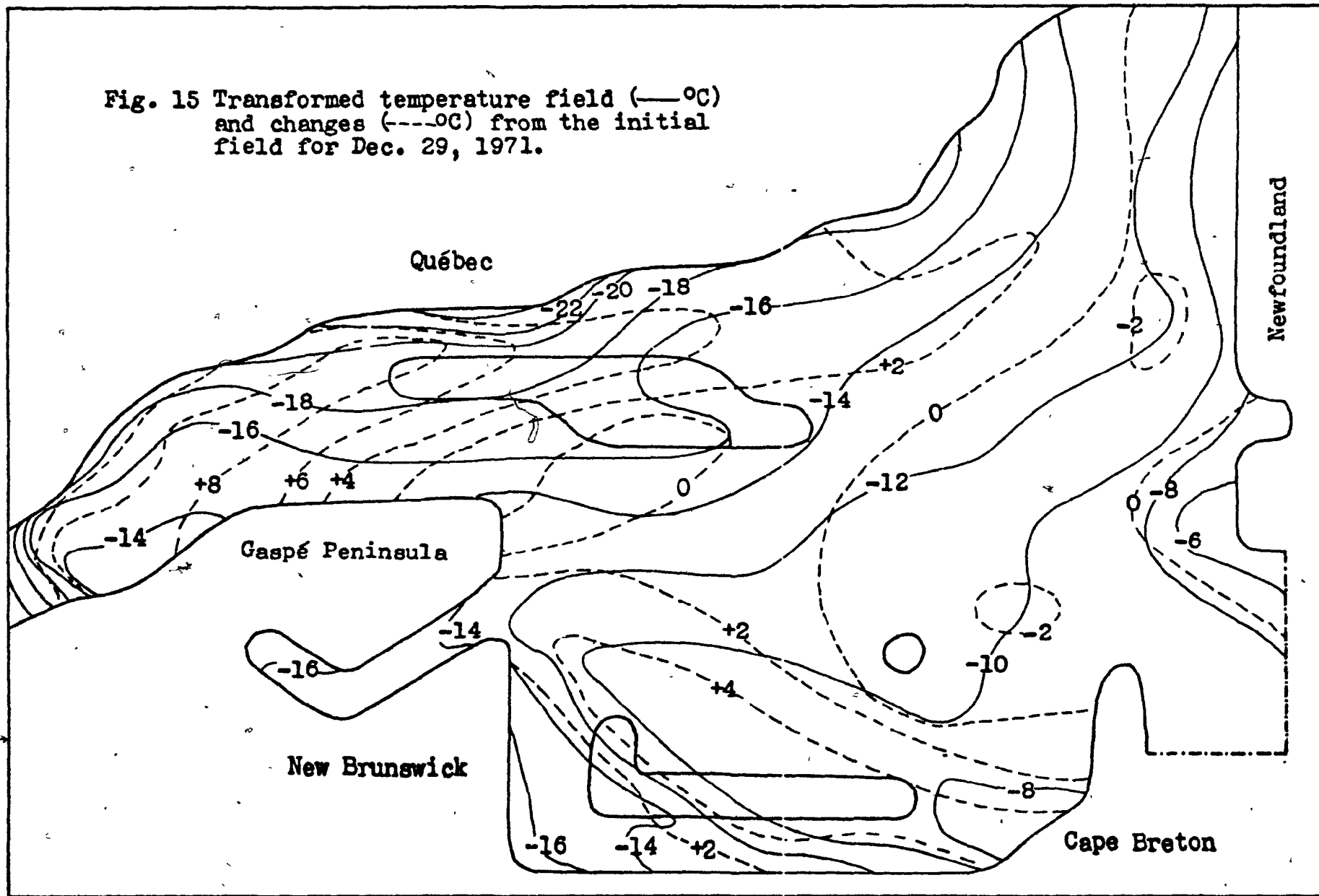
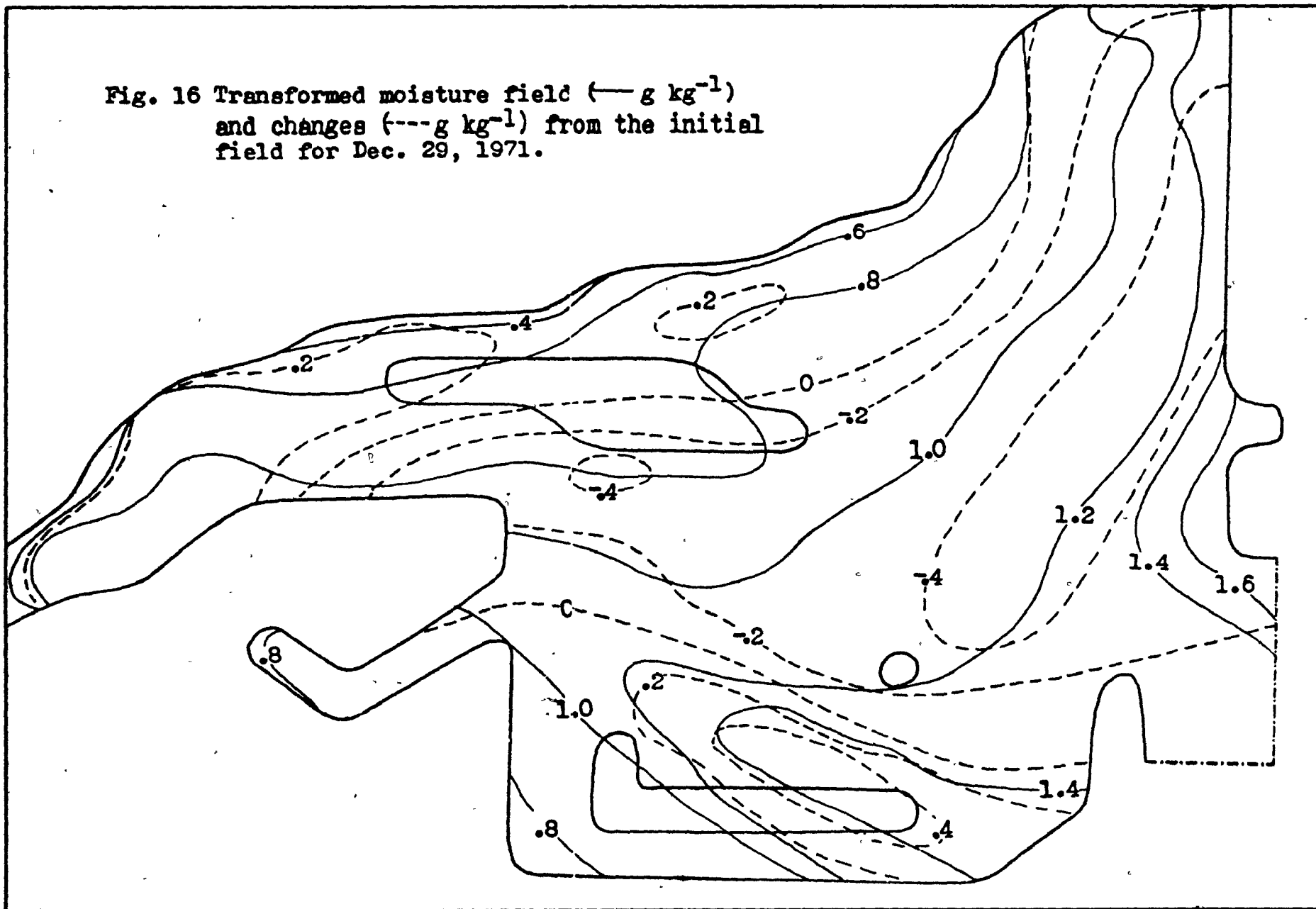


Fig. 16 Transformed moisture field ( $\text{---g kg}^{-1}$ )  
and changes ( $\text{---g kg}^{-1}$ ) from the initial  
field for Dec. 29, 1971.



and moisture profiles were more reasonable than those obtained from interpolated data fields. Cyclonic situations were examined to determine the areal extent and magnitude of modification. The effects exerted by the Gulf on shore line temperature and moisture profiles are also examined.

Examination of temperature and moisture fields during anticyclonic situations revealed a general intensification and north-westward shift of the moisture and temperature gradients for an ice free Gulf. For situations involving an ice covered Gulf with many open leads, the gradients became diffused and generally shifted to the major ice leading edge. Figures 15 and 16, corresponding to the pressure pattern of figure 14b, displays the temperature and moisture field after transformation, and the changes from the initial interpolated fields which are similar to that shown in figure 17a. As can be seen, the changes are mainly positive, indicating that interpolation fails to reveal temperature and moisture gradients resulting from rapid modification. Anticosti Island acts as a moisture and heat sink as is seen by the shift in temperature and moisture lines to the south-east of the island. As Dec. 29 is only a few days prior to ice formation, temperature and moisture gradients along the north-west shore of the Gulf are not as intensive as realized, during similar arctic outbreaks a few weeks earlier, over a much warmer Gulf surface. Regions such as the Cape Breton area are still greatly influenced by the long trajectory of air parcels, as is seen by the warm and moist tongue of air shown in figures 16 and 17.

Figures 18 and 19 display the transformed temperature and moisture fields and the changes which occur under a cyclonic circulation such as occurred after an arctic outburst. Figure 20 shows the actual and computed ice field two days before the passage of the cyclone. An air-water body model utilizing only the initially interpolated fields (figure 17a) would have temperature and humidity fields characteristic of an arctic outburst preceding the cyclone passage over the Gulf. Because vigorous lows often move quickly over the region, a time step of 12 hours may not be sufficient to "capture" typical meteorological field representative of the lower level profiles of temperature and moisture. Figure 14d displays the 12 hour motion of such a low pressure system.

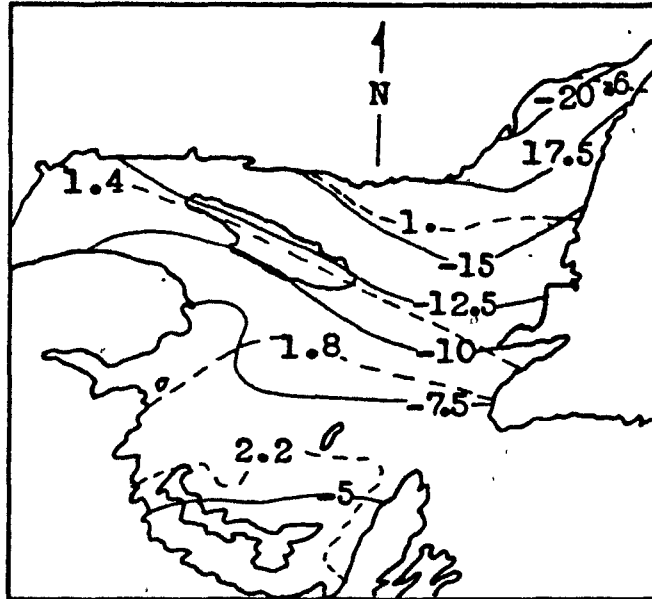


Fig. 17a Interpolated temperature (—°C) and moisture field (----g kg<sup>-1</sup>) for Feb. 4-12Z, 1972.

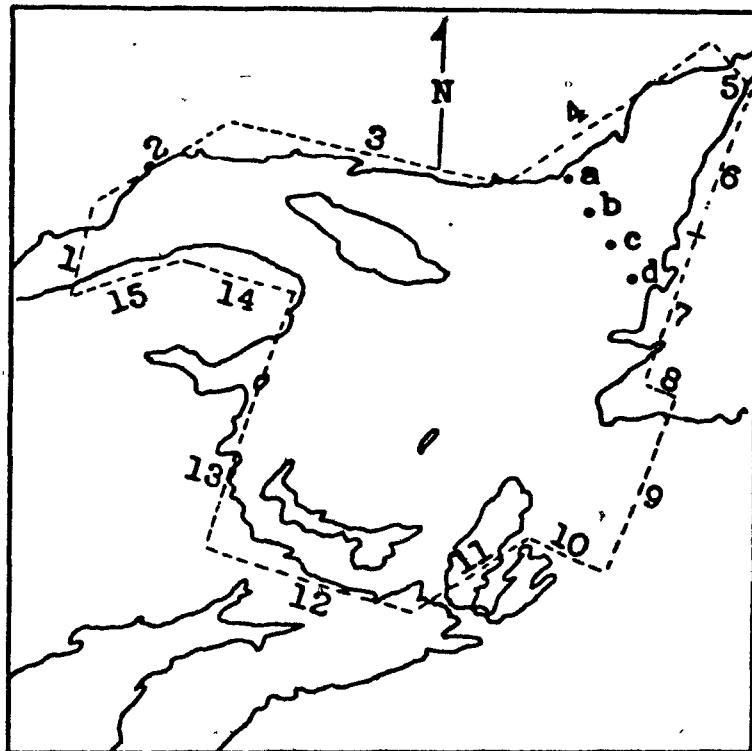
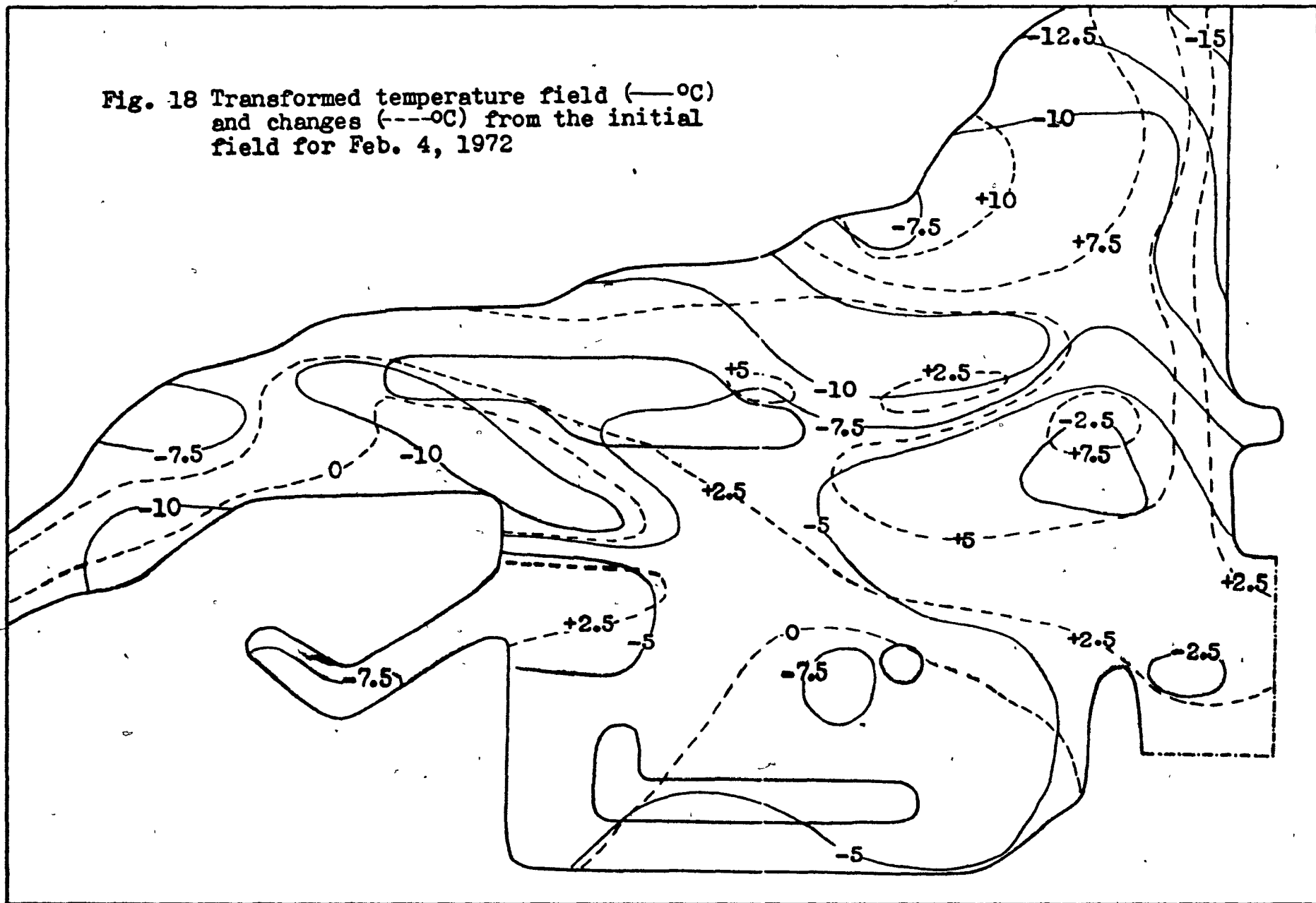


Fig. 17b Polygon used about the Gulf of St. Lawrence in calculating geostrophic fluxes.

Fig. 18 Transformed temperature field (—°C)  
and changes (---°C) from the initial  
field for Feb. 4, 1972



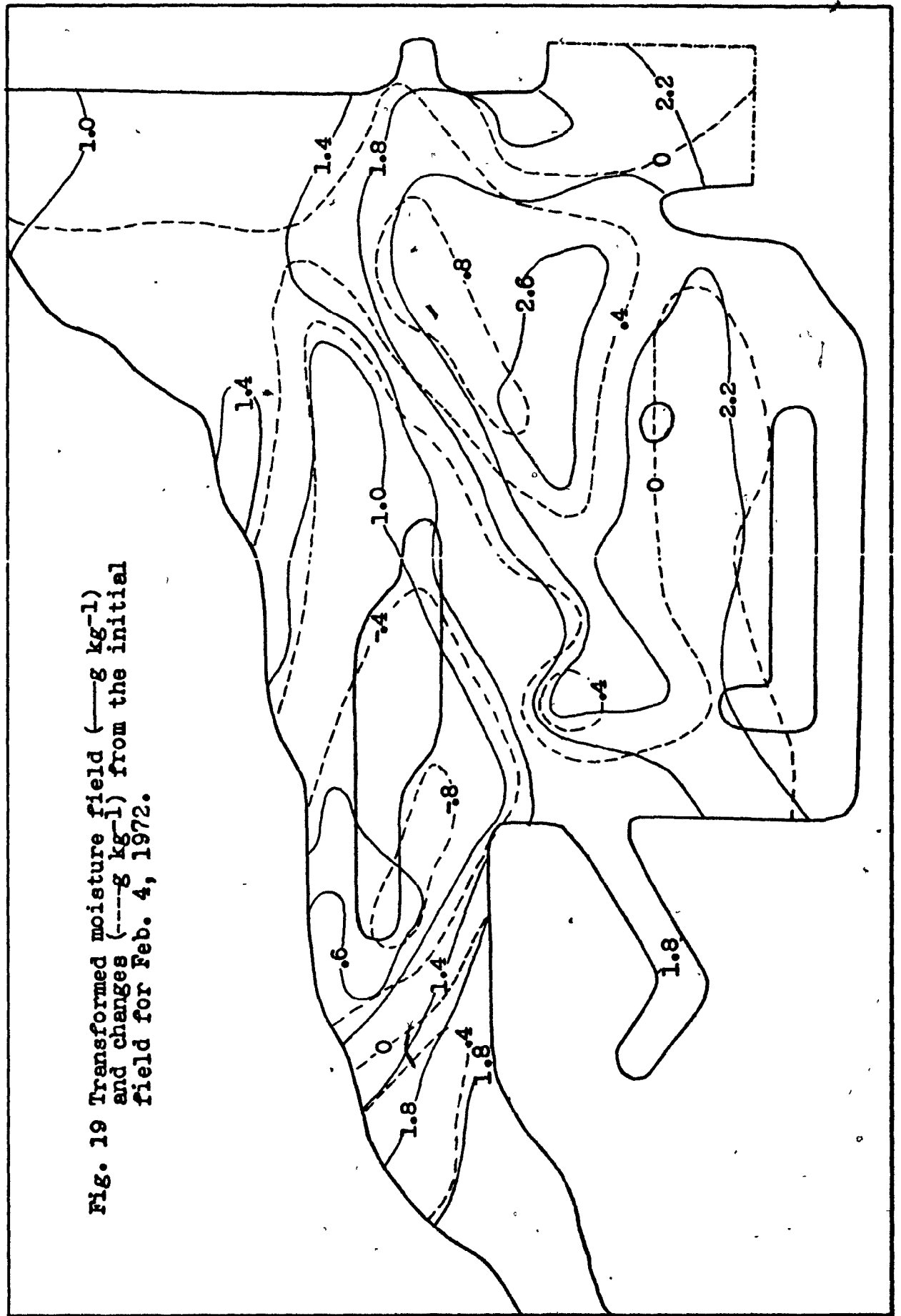
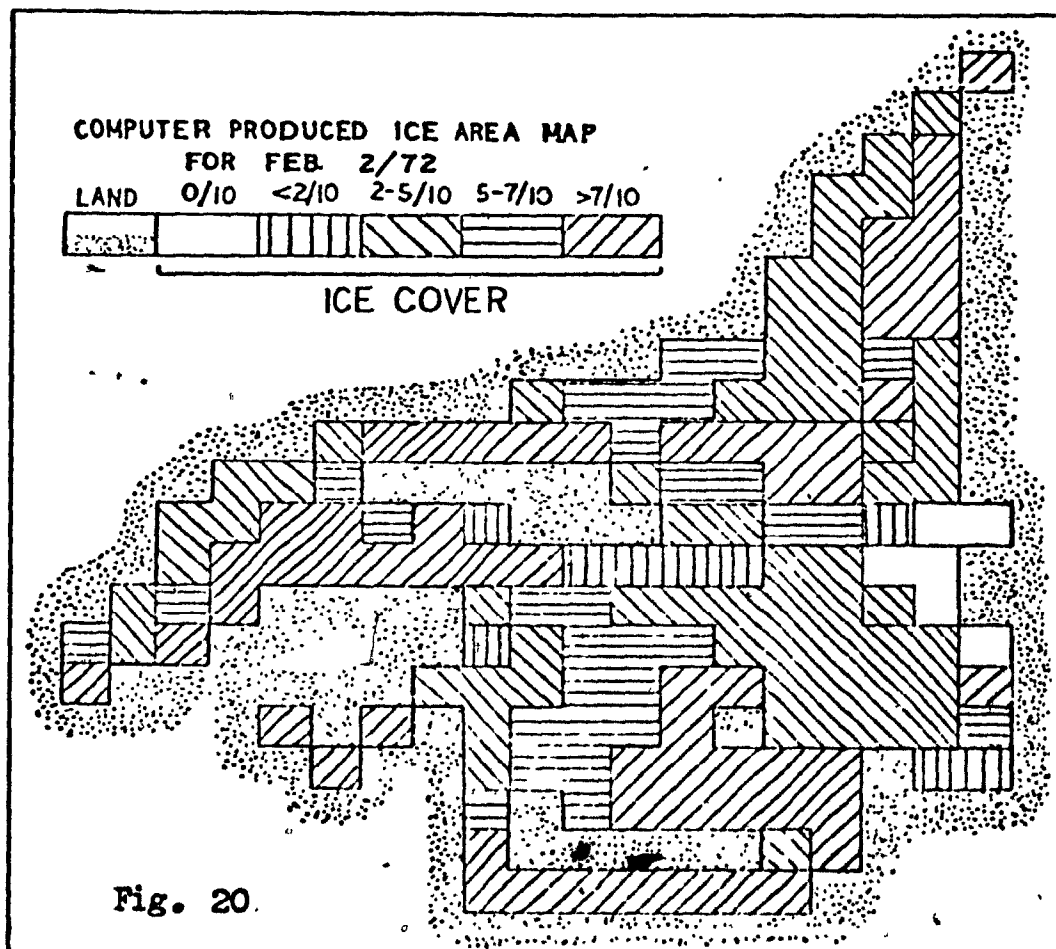
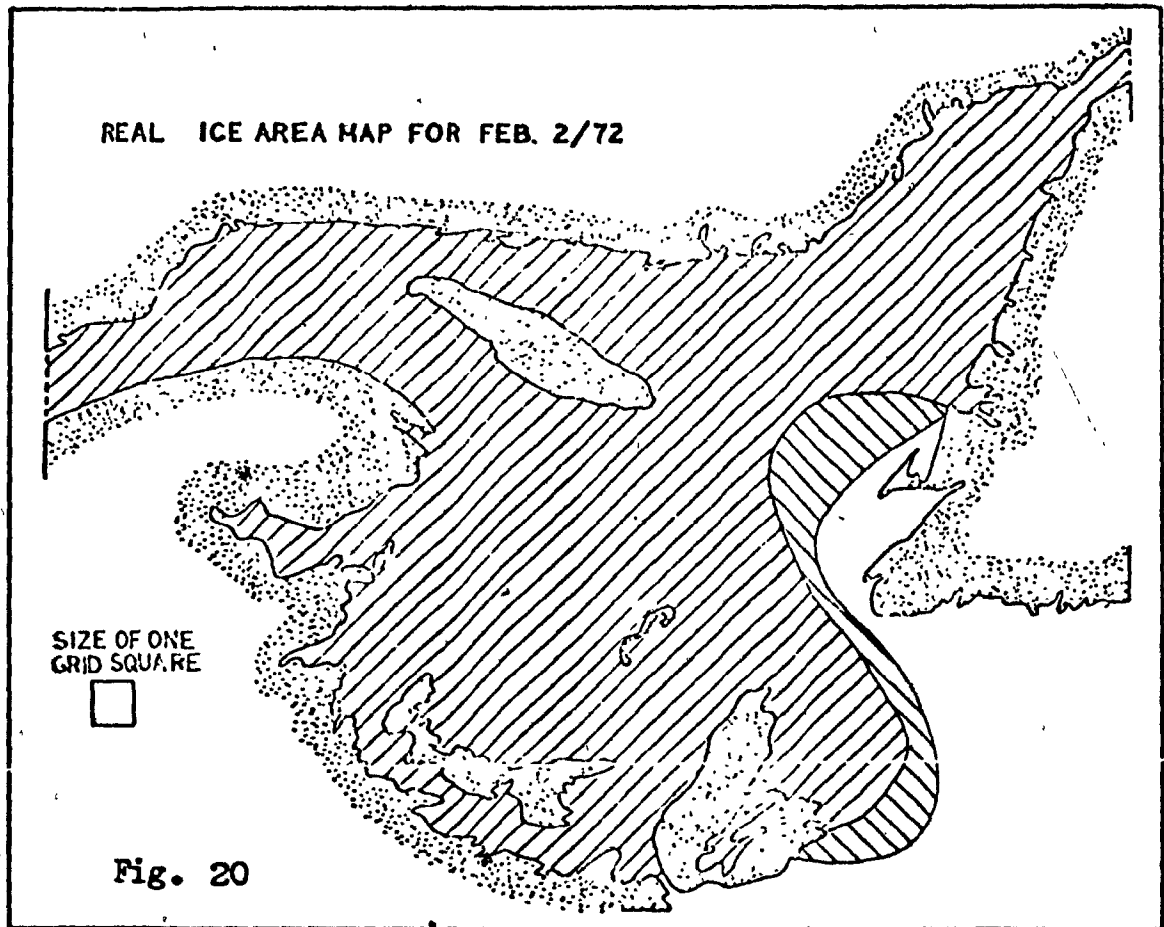


Fig. 19 Transformed moisture field ( $\text{---g kg}^{-1}$ ) and changes ( $\text{---g kg}^{-1}$ ) from the initial field for Feb. 4, 1972.



To neglect modification of the interpolated data field is equivalent to neglecting the effect of intense lows on the Gulf region which tend to decrease flux losses and assuming a general anticyclonic situation which supports higher flux losses. Comparing figure 17a to 18 and 19, the simple temperature and moisture patterns assume a more complicated distribution, partially reflecting the existing ice field with its numerous open leads. In general cyclonic circulations showed modification over a large area. The modification was usually greatest over open water areas. As cyclonic circulations generally have warmer temperatures, temperature and moisture gradients are weaker, thereby having a dampening effect on ice formation.

#### 4.3 Verification

For each time step of 12 hours, redefined meteorological fields were generated by "AIRMTR". An atmospheric model duplicating all physical processes exactly would have final surface parameters identical to those recorded at the end grid points at a later time, corresponding to the transit time of the advected air parcel. Since interpolated fields were only available at every 12 hour period, and since most trajectories are less than 12 hours, the final computed values should lie between interpolated values for the beginning and the end of the period. Shore based reporting stations were used for five situations. For anticyclonic circulations, only four stations were capable of recording representative profiles of temperature and moisture. Because of the higher number of reporting stations along the north shore, seven stations were considered capable of recording representative profiles during situations marked by cyclonic circulation.

In the three anticyclonic situations (see figure 14a, 14b, 14c) the temperature departed from the 12 hour mean by about  $1.1\text{ C}^{\circ}$ . With respect to humidity, the mean departure was  $.15\text{ g kg}^{-1}$ . In both cases, 64% of the final values were within  $1\text{ C}^{\circ}$  and  $.1\text{ g kg}^{-1}$  of the reported temperature and humidity. The largest variation was one case where there were departures of  $3\text{ deg C}$  and  $.35\text{ g kg}^{-1}$  from the mean. The departure may be due to any number of factors, as discussed in sec. 4.1.1. In the cyclonic situation, the time step failed to capture the deep cyclones and good verification is not to be expected. The mean temperature and humidity departures from the

12-hour mean were  $5^{\circ}\text{C}$  and  $.7 \text{ g kg}^{-1}$ . The greatest departures were recorded at the station<sup>5</sup> along the north shores of the Gulf.

In all five situations, it is interesting to note the actual wind field (figure 14). In anticyclonic situations, the instability induced by the warm Gulf water results in the wind at the surface being only slightly veered from the geostrophic wind. On-shore winds generally coincide with the geostrophic flow and reported surface parameters reflect temperature and moisture values close to the computed values. In the cyclonic situations, usually characterized by a more stable atmosphere, surface friction and orographic features along the shores result in a strong convergence of the low level winds along the shores. At times the winds are perpendicular to the isobars (figure 14d and 14e). An examination of the wind vector of the north shore stations reveals that several stations have a general off shore wind, as opposed to an obvious on-shore geostrophic wind. This general low level convergence will result in some shore stations recording temperatures and humidities characteristic of an air mass in equilibrium with a colder and dryer land surface. On the other hand, nearby off shore regions would reveal definite modification. This strong low level convergence, combined with the failure of interpolation schemes to "capture" some cyclonic situations, will make verification difficult. Also, it will lead to erroneous energy budgets if the initially interpolated fields are not modified through some appropriate scheme. While verification of on-shore wind region is desirable, verification of off shore wind regions, where modification is most rapid, would be more useful but is impossible. As previously discussed, the rate of modification decreases with distance, and interpolated temperature and moisture profiles over water surface adjacent to on-shore wind regions, do not differ significantly. On the other hand, off-shore regions lying near land areas with off shore winds may have profiles which differ significantly. Verification of the computed temperature and moisture fields in these off shore regions is desirable, but would require on-site observation over the water areas.

#### 4.3.1 Modification of Shore Line Profiles

Figures 21, 22 and 23 represent the surface air temperature and

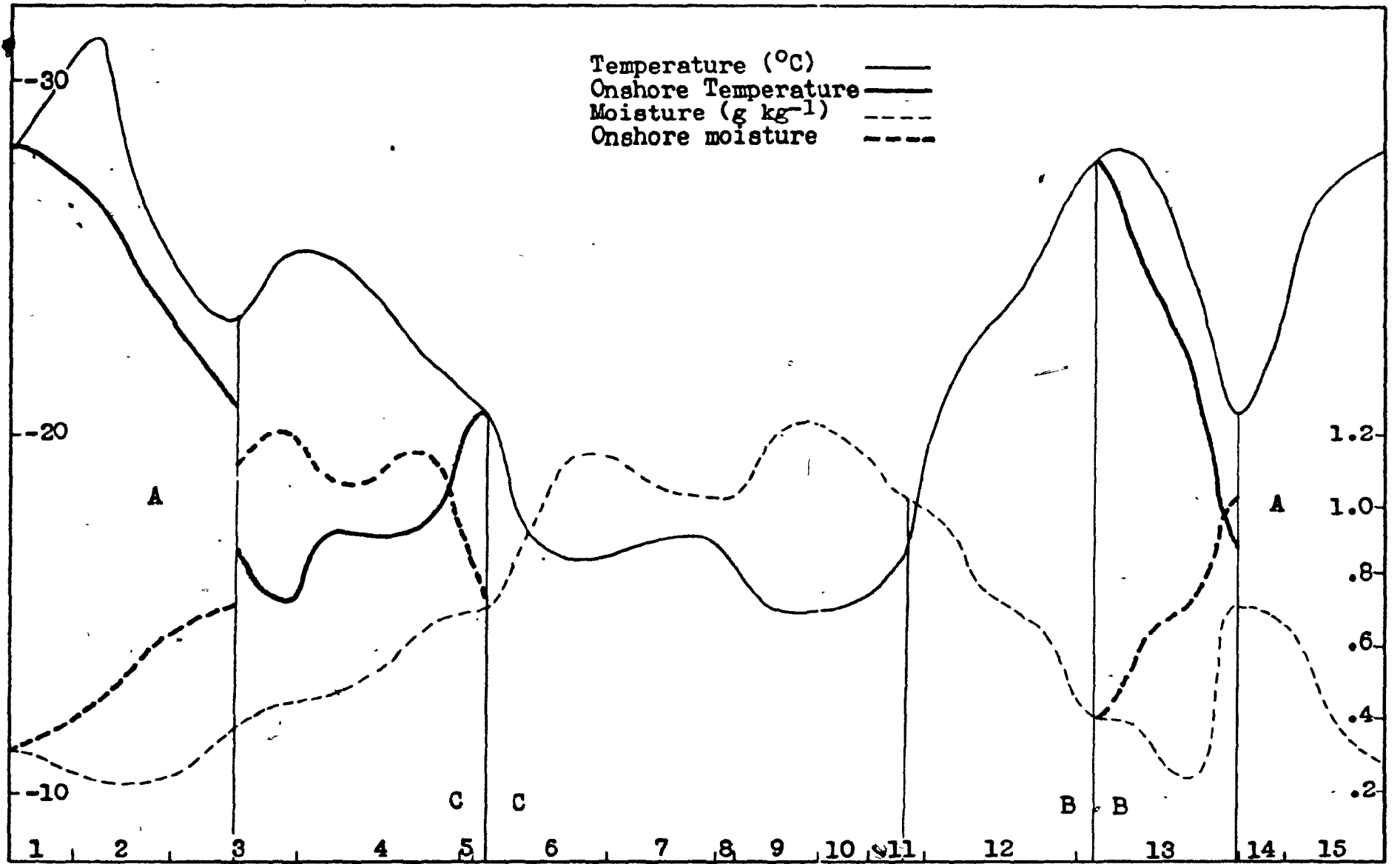


Fig. 21 Surface temperature and moisture profile about the polygon for Dec. 23, 1971.

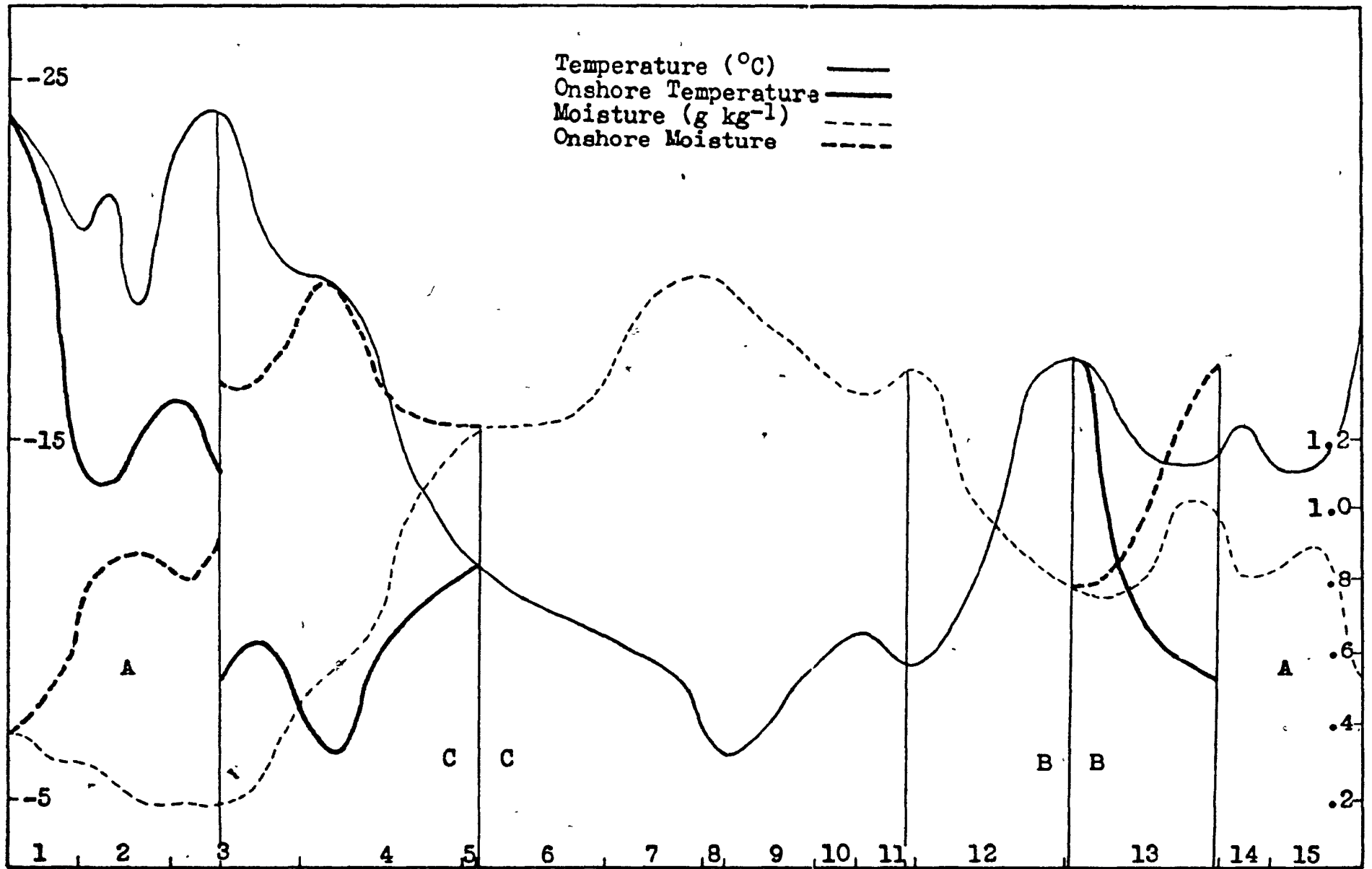


Fig. 22 Surface temperature and moisture profile about the polygon for Dec. 29, 1971.

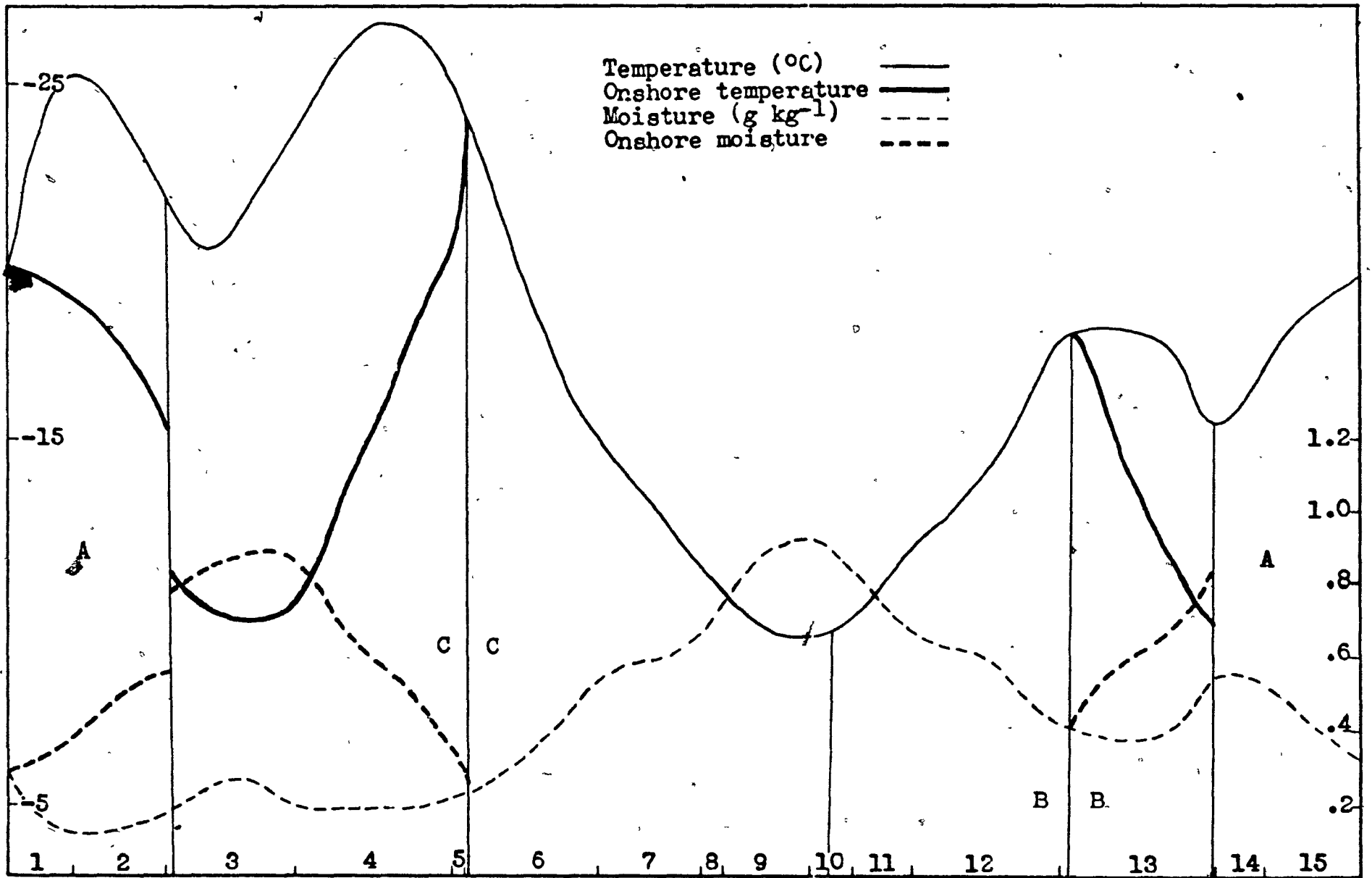


Fig. 23 Surface temperature and moisture profile about the polygon for Feb. 2, 1972.

moisture along the shores, represented by the polygon in figure 17b. The various segments of the polygon are denoted by the numbers at the base of figures 21, 22 and 23. From the flow pattern of figures 14a, 14b and 14c, coastline regions with off shore winds can be mapped on to regions with on-shore winds. As discussed in the previous section, the computed moisture and temperature fields closely represent actual conditions. The continuous solid and dashed lines represent the shore-line temperature and moisture. The shorter underlying or overlying segments represent the corresponding downwind coast-line region. The letters - A, B, C - denote the portion of the coastline which are the on-shore region. Because of confluence in the wind field, the mapped on-shore regions will not be a mirror image. The enclosed areas in these three figures reveal large modification with temperature rises of about 12 deg C and a three fold increase in moisture. The discontinuity in segment 3 of figures 21, 22, 23 results from air parcels leaving segment 2 and 3 (figure 14b), traversing land regions such as the Gaspé Peninsula. They later reappear over the Gulf region with lower temperature and moisture along segment 13 (figure 17b) and still later intercept segments 11 and 12. Meanwhile, other parcels from segment 2 and 3 will bypass the Gaspé Peninsula and continue to segments 11 and 12. Thus, segments 11 and 12 will, under anticyclonic situations as depicted in figure 14, have large temperature and moisture gradients as shown in figures 15 and 16.

The circulation pattern coincident with the shoreline temperature and moisture profile of figure 21 is shown in figure 14a. As previously shown, in section 3.2.1, a high wind speed results in a small residence time and, therefore, modification is not as extensive as in the two other cases shown in figure 22 and 23 under a similar flow pattern. In figure 23, the cold off shore temperatures still experience sizable changes due to the low wind speed (long residence time) and the numerous open leads as depicted by its corresponding ice/water map (figure 20). In the three cases discussed the humidity profile is seen to increase as the temperature increases, indicating that arctic air is not only cold with respect to the underlying Gulf surface but is also dry and capable of absorbing much moisture.

As previously discussed, cyclonic circulations characterized by a south to south-east pressure gradient pattern will result in little or no modified air reaching the northern shore in a manner analogous to anti-cyclonic cases, due to the following two reasons - frictionally induced convergence, and the smaller residence time of cyclonic circulation over the Gulf. As the model is incapable of reproducing the frictional convergence typical of vigorous cyclonic circulation, it is difficult to determine the extent of modification by the Gulf to onshore flow regions. However, for the two reasons stated above, it would be significantly less than the modification occurring under anticyclonic situations. As the shore line grid points, for which iterative energy balances are calculated, are chosen to lie about 18 kms off shore, the effects of frictional convergence will be significantly less so that the fields derived by "AIRMTR" under vigorous cyclonic circulations will closely approximate the actual temperature and humidity fields. The interpolated fields on the other hand fail completely to detect gradients in the meteorological fields in all situations.

#### 4.3.2 Water-Body Heat Content

As previously explained, subroutine "AIRMTR" is a summation of numerous trajectories over ice-water surfaces with varying temperatures. As shown in figure 3, the air-water temperature difference changes drastically from the shore under certain conditions and application of "AIRMTR" will produce gradients of surface temperature and humidity. As shown in section 2.1.5, latent and sensible heat fluxes are greatly dependent on the air-sea temperature difference and the distance from the shore line. Diagram 24 shows the heat loss from four points, whose positions are shown on diagram 17b. During periods under north-west flow patterns, the heat gained by an air mass (and lost by a water body) is greater for points nearest the north-west shore of the Gulf. Between Dec. 23rd and Jan. 2nd, the rate of heat loss (indicated by the slope of the curves) generally decreases with the distance from the north-west shore. During cyclonic situations, the change in slope is unnoticeable as one would expect during periods of lesser modification. The cumulative effect of air-mass transformation is reflected in the energy lost by the water body to the atmosphere - up to 1500 calories between points "a" and "d". The difference

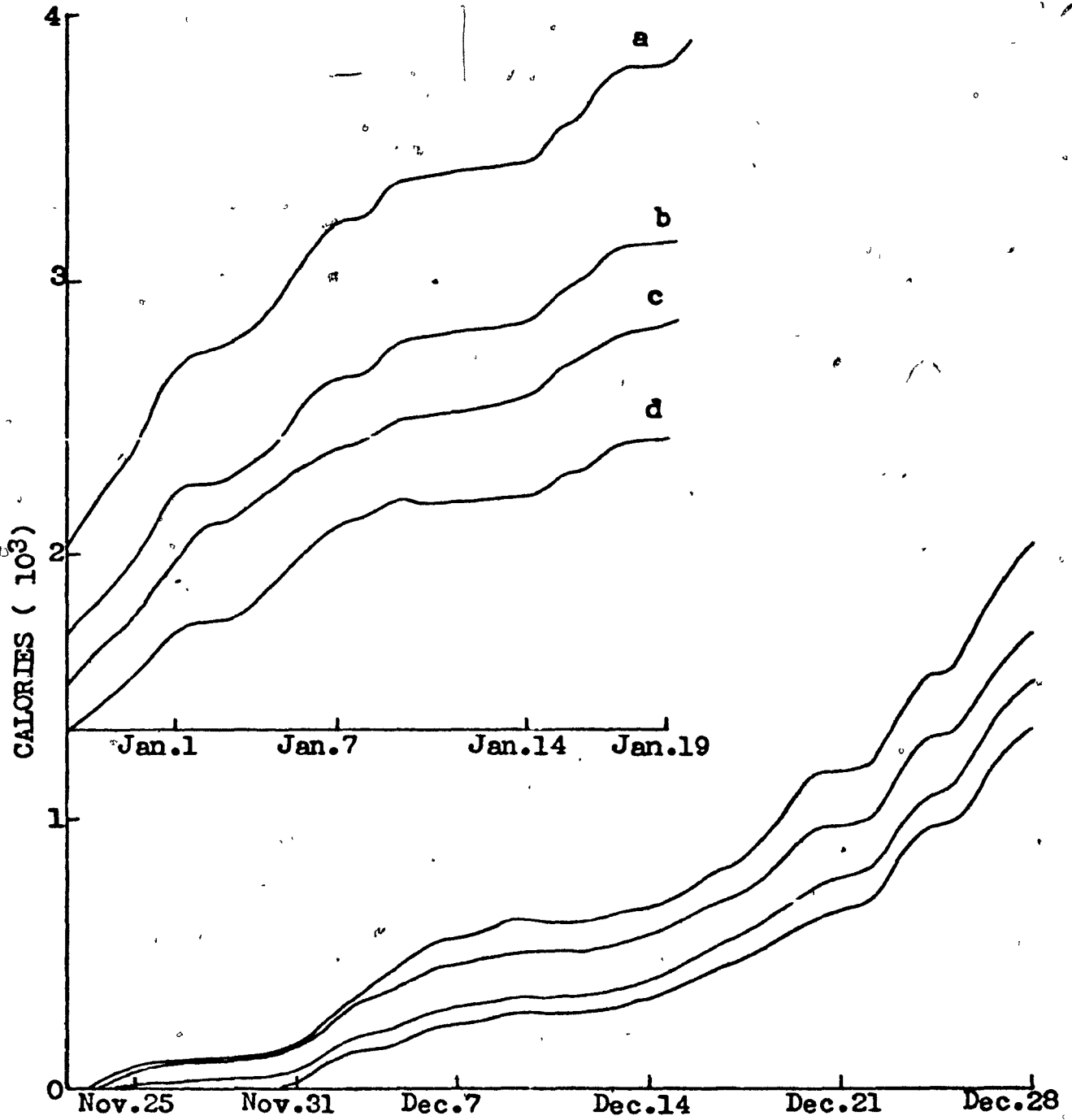


Fig. 24 Recorded heat lost per unit area at four water grid points.

would be greater but for the initially higher temperatures along the west coast of Newfoundland. It is this cumulative effect of initially high exchange rates under arctic outbreaks which allows for ice formation regions generally to occur along the north and west portions of the Gulf. Not modifying the surface air temperatures and humidity by the subroutine "AIRMTR" would result in larger portions of the Gulf acting as main ice production areas. "AIRMTR" basically acts as a redistributing mechanism for the moisture and temperature gradients. It does not affect significantly the total energy of the water body as seen by the initial onset of ice (Lally, 1973).

#### 4.4 Summary

Under anticyclonic situations, "AIRMTR" yields a better low level temperature and humidity profile near off shore regions as well as producing a representative surface temperature and humidity field for on shore regions. Under cyclonic situations characterized by a fast moving cyclone over the region, "AIRMTR" generates a more representative temperature and humidity field over the entire Gulf area.

An iterative process such as "AIRMTR" would definitely result in larger ice formation regions and radically different ice fields. The desired resolution in ice fields determines to a large extent the need for "AIRMTR". If only a "yes" or "no" answer is wanted, as to whether or not ice forms over the Gulf, then one grid point at the center of the Gulf would suffice and "AIRMTR" could be omitted.

#### 4.5 Water and Energy Budget Analysis

From section 2.1 and 2.2, the sensible heat and moisture budget equations for an enclosed vertical air column is given by

$$\Delta SH = F_{SRQS} + PCPN + QSADV$$

where  $F_{SRQS}$  incorporates the radiative terms and the sensible heat flux exchanged.

$$ALH = QE + QEADV - PCPN$$

The following terms summed over a portion of the period under study will be examined to determine the reliability of the advective term as obtained by using the geostrophic wind.

#### 4.5.1 Precipitation - PCPN

The interpolated field of precipitation for case 1 and 2 combined (Table 3) gave a value (per unit area) of 3.9 and 2.7 inches, respectively. For the same period, Summerside and Charlottown reported 5.1 and 8.9 inches respectively - the stations being only 30 miles apart. Orographic and local turbulence definitely have influences on the recorded precipitation. Since numerical analysis areally weighs each data point, the influence of orographic effects will diminish. For the same period the mean precipitation as computed from the Canadian Monthly Weather Review is 3.5 and 2.9 inches. If error in the data were eliminated, the precipitation as numerically analysed would be more accurate. The basic error lies in determining the latent heat released which is determined by the type of precipitation and can be incorrect up to 13% (see 2.1.6). However, since the latent heat is about 10% of the total energy exchanged, the significance of this error is considerably diminished.

#### 4.5.2 Storage Term

Because of the isobaric mass associated with a synoptic system changes with time, the energy and water budget equations (equations 1 and 2) must account for the storage change which occurs during the period under analysis. As the length of the period increases, the significance of the storage term decreases. From Table 3, the changes in storage of sensible heat (STSH) and moisture (STLH) are of the same order of magnitude as the other terms for periods of a few days and become insignificant when the period under analysis extends over several weeks.

The change in storage of a quantity "J" was calculated by the following method:

TABLE 3  
 COMPONENTS OF SENSIBLE HEAT AND MOISTURE  
 BUDGET EQUATIONS (LY DAY<sup>-1</sup>)

	<u>TIME PERIOD</u>	<u>CIRCULATION TYPE</u>
1.	Dec. 2-00Z to Dec. 23-12Z	mixed
2.	Dec. 24-00Z to Feb. 02-12Z	mixed
3.	Dec. 24-00Z to Dec. 28-12Z	mixed
4.	Jan. 04-00Z to Jan. 06-12Z	anticyclonic
5.	Jan. 07-00Z to Jan. 14-00Z	cyclonic
6.	Jan. 22-12Z to Jan. 26-00Z	cyclonic
7.	Jan. 26-12Z to Jan. 30-00Z	anticyclonic

	QE	PCPN	STLH	QADV(C)	QADV(B)
1.	196	193	-15	-176	-18
2.	185	173	-3	-132	-15
3.	294	265	42	344	13
4.	256	89	-65	-583	-232
5.	104	161	96	138	153
6.	83	319	-36	376	200
7.	206	79	-16	-244	-143

	FSRQS	QS	STSH	QSADV(C)	QSADV(B)
1.	75	290	-72	-611	-340
2.	158	334	-19	-1300	-350
3.	409	574	258	52	-416
4.	256	442	-331	4040	-676
5.	-103	146	301	155	243
6.	-218	59	-364	1149	-465
7.	457	624	-95	-2532	-631

$$\Delta J = J_2 - J_1 + \Delta P_2 / \Delta P_1$$

where  $J_1, J_2$  = storage at time  $t_1$  and  $t_2$  respectively,

$\Delta P_1, \Delta P_2$  = pressure difference between the surface pressure and 150 mb (850 mb for moisture calculations) at time  $t_1$  and  $t_2$  respectively.

The isobaric mass correction in the case of moisture storage calculations is confined to below 850 mb as between 25% and 50% of the moisture is held in this region where most of the moisture changes occur. The 150 mb level was taken as the upper level as no information was available for higher region. In general, the atmosphere experiences little change at this high level.

#### 4.5.3 Latent and Sensible Heat Fluxes

Since the flux exchange equations were developed by analysing data over large time periods with varying synoptic conditions, QE and QS as calculated by the air-water body model will tend to give a reasonable estimate. This is revealed by the ice formation occurring in critical areas such as Bay of Chaleur and the Northumberland Straits on the reported dates (Lally, 1973). Like the precipitation term PCPN, QE and QS as well as the change in storage of these two terms can be used with equal confidence in the energy and water budget calculations.

Table 3 reveals the magnitude of QE and QS under varying type of circulation patterns. In cases 1 and 2, the long time period<sup>5</sup> involved do not result in daily exchange rates that differ significantly; however, between case 4 and 6 the exchanges vary by a factor of 3 for latent heat and 8 for sensible heat. It is this sharp variation in the flux exchange over a short time period which results in rapid and critical changes of surface parameters such as water temperature and ice formation. Calculations for cases 4 and 7 reveal greater exchange rates for anticyclonic situations than for cyclonic. This correlates with the fact that anticyclonic circulations during this winter period involve colder, dry air mass<sup>6</sup> capable of greater modification.

It appears that flux exchange calculations for 12 hour periods are sufficient to reveal the time variations in flux exchange rates associated with synoptic scale events having a cycle time of 2 to 4 days.

#### 4.5.4 Radiative Terms

The radiative terms consist of the following: RLU, DFL, UFL, SAA. The term SAA is the least affected by incorrect estimates of cloud amounts and heights. As for the other three terms, the largest errors would be attributable to incorrect temperatures, cloud amounts, and heights. As discussed in section 4.1, the significance of spurious errors in the temperature, cloud amount and height field will be greatly reduced and the estimated radiative terms will be reasonably accurate. In Table 3, the term SRQS is the sensible heat gain attributable to the radiative terms and QS (the sensible heat gain from turbulent exchange). Examination shows that the atmosphere continually loses energy by radiation.

#### 4.5.5 Advective Terms

Although Benton and Estoque (1954) were able to estimate correctly the advective terms of water fluxes over a period of several months over North America, Palmén and Soderman (1966), in doing an analysis of the water budget over the Baltic Sea, concluded that using geostrophic flux would give overestimates of the outgoing fluxes. Bradbury (1957) arrived at a similar conclusion. In the study undertaken over an area similar to the Baltic Sea area, the present author concludes that using geostrophic winds tends to give a large overestimate. This is shown by the computed advective terms denoted by (C), and their values as derived from the balance of the energy budget denoted by (B), of Table 3. From the advective term, the geostrophic flux of vapor "q" can be represented by the following equation:

$$QEADV = \frac{1}{g} \int_0^{p_0} \bar{v} \cdot \nabla q \, dp$$

whilst the geostrophic contribution is

$$QEADV^* = \frac{1}{g} \int_0^{p_0} qV \cdot \vec{V} dp$$

In cyclonic circulation, the relative humidity is usually much higher than in anticyclonic cases. Neglecting the ageostrophic term, therefore, tends to overestimate QEADV. Similarly, QSADV will be overestimated (see cases 1 and 2 of Table 3). Examination of any period during which the Gulf has a strong cyclonic circulation will reveal strong convergence of the surface winds. As the layers of greatest moisture content <sup>are</sup> ~~is~~ located in the lower regions where surface friction is greatest (1000 to 2000 m above ground) the assumption of geostrophic winds will lead to overestimates of actual net flux exports. In anticyclonic cases associated with polar outbreaks, general instability results in winds which tends to be near the geostrophic wind direction and speed, and since the moisture content is low, the error in assuming geostrophic winds will be less. For the period under study, an overestimate of about  $1000 \text{ cal cm}^{-2} \text{ day}^{-1}$  of sensible heat and  $150 \text{ cal cm}^{-2} \text{ day}^{-1}$  of latent heat resulted from using geostrophic winds. In terms of isobaric mass, this represents a mass export of about 15 mbs  $\text{day}^{-1}$  for air assumed to have a mean temperature of  $260^\circ\text{K}$ . Similarly for moisture, this represents a mass of about .25 grams of moisture leaving the Gulf per day. Assuming a mixing ratio of  $1 \text{ g kg}^{-1}$ , a daily export of 15 mb would result in a loss of about .015 grams of water (about 15 times less than computed from geostrophic fluxes). This discrepancy is due to the horizontal and vertical humidity gradient in the lower 150 mbs which is much greater than the temperature gradient, and with convergence greatest near the surface boundary, the errors in assuming geostrophic flux of moisture will be larger than the geostrophic flux of sensible heat.

Since the geostrophic flux overestimates a sensible heat export by  $15 \text{ mb day}^{-1}$ . This implies a convergence of sensible heat as well as moisture due to the ageostrophic wind. Since frictional convergence is confined to the lower 1000 to 2000 m of the atmosphere, this results in a vertical velocity above the friction layer of about  $1 \text{ cm sec}^{-1}$  over the 63 days using the approximation that 1 mb represents a thickness of 10 meters near the surface.

If the geostrophic fluxes were assumed correct, the energy budget

equations would require latent and sensible heat exchanges to increase by a factor 2 and this would in effect, result in much earlier ice formation. In situations such as described in sec. 4.1.1, where cold arctic outburst were examined, the maximum amount of latent and sensible heat gained was  $80 \text{ cal cm}^{-2} \text{ hr}^{-1}$  which compares favorably with the extremes encountered by Craddock (1951).

In the program, the amount of liquid water advected was recorded in order to estimate the proportion of total advected moisture attributable to cloud export. In the water budget, the mass of liquid water associated with cloud advection is 20% of the total water exported (vapor plus liquid) in the case of polar outbreaks. Under cyclonic situations, the liquid water is 27% of the total water advected. Since the advection was determined by using geostrophic winds, the use of actual winds might reduce the contribution of clouds to the total liquid water export for the following reason: the actual wind convergence and, to a lesser degree, cloud distribution, varies with distance from the ground, and the flux would thus be modified. The reason for such a high contribution of clouds is the relatively small humidity of dry arctic and maritime polar air. During the summer season, when the water holding capacity of air is much greater, the contribution of clouds would decrease. Ninomiya (1968) concluded that the condensed water transport did not exceed 10% of the water vapor. Because the water body region under study here had a much higher surface temperature than the Gulf surface, the temperature modification was more extensive. The capacity to hold water vapor increases while the cloud liquid water content does not change appreciably in this temperature range.

#### 4.5.6 Energy Disposition

Since energy budgets (equation 2) are less susceptible to errors the longer the time period involved, and since the storage term becomes negligible, the percentage contribution of each term to the total sensible heat energy involved can be estimated (Table 4).

TABLE 4  
COMPONENTS OF THE SENSIBLE HEAT BUDGET (%)

STSH	SAA	PCPN	QS	UFL	QSADV	DFL	RLU
=0	+2	+8	+13	-14	-14	-22	+27

The long wave radiation emitted (RLU) from the total Gulf surface is roughly  $.9 \times 10^{21}$  calories over the 63 day period. From Table 4, the sensible heat is roughly 50% of RLU. However, the net gain to the atmosphere is much less when one takes into account the outgoing radiation which thereby results in a net loss of about 7%, almost equally compensated through the precipitation term. From the advection term, we see that there exists definite export of sensible heat from the Gulf region of the same order as the heat gained from sensible heat exchange over the Gulf surface. Were it not for the presence of the warm Gulf water surface, the contribution of the sensible heat from PCPN and QS would be less. As the radiation term would not change as drastically as PCPN and QS, the advective term would definitely decrease and could possibly reverse sign, indicating a net flux import in the assumed "non existent Gulf region".

The Gulf does have a significant effect on air masses passing over the region in winter. Heat stored by the water body is later released through evaporation and subsequent condensation, and through sensible heat exchange. It is this exchange which has a definite recognizable effect on on-shore temperature and humidity profiles as shown by the surface temperature and humidity profile plotted for a polygon about the Gulf coast (see figures 21, 22, 23) and for an individual vertical profile - figure 11 and 12.

## CHAPTER V

## CONCLUSION

Oceanic areas are generally characterized by weak temperature and moisture gradients as well as near geostrophic wind conditions throughout the vertical. On the other hand, small water bodies such as the Gulf of St. Lawrence, which possess a finite heat supply, will be characterized by strong temperature and moisture gradients during the winter season.

A method was described to adjust and determine the intensity and location of the parameters essential in the formation of annual ice fields, and not available by simple interpolation of meteorological data. Because of the time steps involved, the representativeness of recorded and adjusted fields will be greatly dependent on the persistence of the atmospheric circulation pattern over the area.

The orographic convergence induced by the high terrain surrounding water bodies such as the Gulf region will seriously reduce the validity of calculated geostrophic advection of sensible and latent heat. The direct calculation of the advected fluxes could be possibly accomplished by the introduction of more radiosondes with their corresponding wind profiles about the Gulf. A more realistic and economical approach is an estimate obtained from a budget analysis whose principal terms are more accurately determined either through increased surface observations over the Gulf or smaller time step intervals.

## APPENDIX A

## DESCRIPTION OF WATER BODY PROCESSES (LALLY, 1973)

2.9 The Balancing of the Surface Energy Budget

(b) The radiation balance of the budget over an ice or snow surface is carried out in subroutine "YEW", which is equivalent to Vowinkel and Orvig's "LEDA", (VO72). It is an iterative process which alters the ice/snow surface temperature in the appropriate direction until the radiation balance becomes sufficiently small, (must be  $\leq 10 \text{ cal cm}^{-2}$ ).

2.10 The Water Processes and Their Reaction to the Surface Energy Budget

(a) A body of water is constantly reacting to the surface energy balance. If there is a deficit of heat at the surface the water must give up heat, which it contains in storage, in order to balance this deficit. The processes by which this heat may be brought to the surface are thermohaline connection in reaction to a density gradient rendered unstable by the surface cooling. Secondly, if the water experiences turbulent motion due to wind stress heat is also transported. In the absence of these two phenomena, molecular heat conduction must serve. In the case of a surplus of heat at the surface, the amount of heat in storage in the water may be augmented if processes exist to transport that heat downward. Turbulent motion and molecular heat conduction are two obvious processes which could accomplish the downward transport of heat. Thermohaline convection, on the hand, would require a simultaneous rise in salinity to give a downward transport as this would help overcome the increased stability of the density structure due to surface warming. Finally, a second reaction results from a heat deficit at the surface, that is the formation of ice. Ice will form if the heat deficit is sufficiently large to lower the surface temperature below its freezing point and no heat is available from below to rectify this deficit.

The processes thus far mentioned which transport heat are:

- (i) Molecular heat conduction
  - (ii) Thermohaline convection
- and (iii) Dynamic convection (turbulent mixing).

The time scale of these processes must be examined to ascertain which are significant. Considering molecular conduction first, Defant (De61) shows that the time for one half the magnitude of a surface temperature change to reach 1 m is on the order of  $\frac{1}{4}$  of a year and to reach 10 m, 27 years. This means that the other two processes are orders of magnitude faster in transporting surface heat anomalies. Thermohaline convection is on the order of hours and dynamic convection if not quite as fast is only slightly slower, possibly on the order of days. Thus, with negligible error molecular conduction may be neglected as a significant water body process. Absorption of solar radiation, brine migration, and flooding of the ice when the snow cover becomes thick.

#### 2.12 Dynamic Convection (turbulent mixing)

(a) Dynamic convection is a turbulent process caused by the stresses set up in the water body as wind blows across the surface. The resultant disordered eddying causes quanta of water to move and thence become mixed. Turbulence is a dissipative phenomenon, the dissipation being caused by work being done against the viscous forces in the fluid. The dissipative effects of the fluid are larger if the fluid is stably stratified in its density structure.

In a stably stratified fluid the regimes of turbulent and non-turbulent motion are separated by a sharp interface, which is gradually broken down as entrainment of non-turbulent water takes place. In this case the turbulence does work to overcome the buoyancy created by the stability of the fluid. If sufficient energy is available for the creation of turbulent motion, then a mixed layer of water forms. It is this mixed layer which creates a heat storage facility in the water body. Finally, the depth of the mixed layer is dependent upon two things: first the amount of negative buoyancy force available for mixing and, second, the magnitude of the buoyancy forces that must be overcome. The amount of negative buoyancy force is a function of the wind force and the duration of that wind. The buoyancy forces are a function of the density gradient and thus depend upon water temperature and salinity.

(b) The simulation of dynamic convection considers both the turbulent energy made available to the water and the stability structure. The latter however, does not consider the density explicitly as in fact the temperature only is used to determine the stratification of the water body.

The scheme used is derived from empirically derived curves of the Royal Navy (Anon68). These curves were derived from three years of observations at the weather ships 4YI and 4YJ in the Northeast Atlantic ocean.

### 2.13 Thermohaline convection

(a) Thermohaline convection is simply the reaction of the water to an unstable density gradient. It can be triggered in two ways (i) the surface water becomes colder and hence more dense (in sea water with salinity  $> 24.7^{\circ}/\text{oo}$ ) and (ii) the surface water becomes more saline. This is true of lower layers as well and, of course, any combination of (i) and (ii) may have similar effect.

Cooling of the surface layer occurs most often in the fall when colder air begins to pass over the water, reducing the heat storage there. An increase in salinity readily occurs when ice forms on the water, dropping out brine into the water and making it more dense. There are two additional processes which affect the surface density, namely precipitation and evaporation. Both these processes act through the salinity, making the surface layer either less or more saline.

(b) This process is easily simulated given temperature and salinity profiles. It amounts to comparing the density of any lower layer with the layer above. If there is instability the layers will be mixed, if not no mixing occurs. Only surface cooling and salinity increase due to ice formation are considered in the program. Precipitation and evaporation are considered to be too small to affect the system significantly. This is easily seen if a centimeter of water is evaporated and that water's original salinity is  $30.00^{\circ}/\text{oo}$ , then the top layer of water in the model, being 250 cm, undergoes a salinity increase of  $0.03^{\circ}/\text{oo}$ . When these salinities are initially put into the model they are accurate to only  $\pm 0.10^{\circ}/\text{oo}$ ,

so the increase of  $0.03^{\circ}/\text{oo}$  is below the allowable error. The process takes place in subroutine "OAK".

#### 2.14 Ice Formation and Build-up

(a) The constant removal of heat from the water body experienced in the fall months eventually results in the depletion of available heat for surface layer warming. At some point the heat supply becomes insufficient to keep the water open and the result is the formation of an ice sheet. After ice forms, heat is conducted through it causing more ice to form on the underside of the existing sheet. With the onset of warmer spring weather the ice will melt from above and eventually disappear. During the winter, heat may have been trapped in the water below but remained unavailable for surface warming due to a stable density structure. Then, as the salt from ice formation is dropped in the water the density structure becomes unstable and the overturning causes the heat to rise and thus melts the ice from below. In these ways the ice will form, grow and decay.

#### 2.16 Flooding of Ice and the Resultant Snow Ice

(a) When the weight of the snow cover lying on the ice becomes sufficient the ice surface becomes submerged. The resultant flooding causes the snow and sea water to mix and form a layer of snow ice above the existing ice layer.

#### 2.17 The Horizontal Processes

(a) Possibly the most important horizontal process in an area such as the Gulf of St. Lawrence is the water movement due to the currents. These currents transport heat and salt and ice when it is present.

To the author's knowledge no detailed picture of the subsurface current pattern of the Gulf area exists. Further, there is no detailed knowledge of the depth to which the surface currents extend.

One essential process which can be included is ice advection, as this requires only knowledge of the surface current pattern. Thus, ice advection has been included in the model. The current pattern used for

this purpose is based on Trite's summer current pattern which is assumed constant over the entire year. This assumption is probably erroneous, but is the best available.

The effects of both wind and currents on the drift of ice are used to advect that ice in subroutine "WILLOW". The wind is used to drift the ice at 2% of the wind speed and in the direction of the isobars, after Zubor (Zu43). The ice also drifts with the current at its own speed. No provision is made for the deflection of the ice from geographic al barriers due to the deflection of the wind. A further constraint is that the ice is not allowed to move more than 37 km in one day, though it may move less. This is a computational criterion as the grid length is 37 km.

In a grid square model of this type a distinct ice edge may not be represented as such. If an ice edge moves into an area to cover five tenths of the area, then the entire area is considered to have five tenths ice coverage for each unit area, no matter where it is located. This means that ice from grid square may advect into the next one, in the program, which would not happen in reality unless conditions specifically allowed it. This is to say that the program may suffer from spurious ice advection. To overcome this a criterion is introduced which does not allow ice to advect from a given grid square until that grid square contains at least two tenths ice coverage. One further comment is due; though the ice is allowed to pile up on windward shores, all ice has an average thickness over the entire square as does the snow cover over the ice.

## BIBLIOGRAPHY

- Benton, S.B., Estoque, M.A., 1954: "Water Vapor Transfer over the North American Continent". J. Meteor., Vol. 11, pp. 462-477.
- Burbidge, F.E., 1951: "The Modification of Continental Polar Air Over Hudson Bay". Q.J.R.M.S., Vol. 77, pp. 365-374.
- Bradbury, D.L., 1957: "Moisture Analysis and Water Budget in Some Non-developing Cases". Geophysica, Vol. 6, pp. 179-187.
- Burke, C.T., 1945: "Transformation of Polar Continental Air to Polar Maritime Air". J. Meteor., Vol. 2, pp. 92-112.
- Coombs, J.A., 1962: "A Preliminary Investigation of the Heat Budget in the Gulf of St. Lawrence". Bedford Institute of Oceanography, Report B.I.O. 62-1, Oct. 62, 50 pp., (Unpubl.)
- Craddock, J.M., 1951: "The Warming of Arctic Air masses over the Eastern North Atlantic". Q.J.R.M.S., Vol. 77, pp. 355-364.
- Craig, R.A., 1949: "Vertical Eddy Transfer of Heat Water Vapor in Stable Air". J. Meteor., Vol. 6, pp. 123-133.
- Danielson, E.W., 1969: "The Surface Heat Budget of Hudson Bay". Marine Scientists Manuscript Report No. 9, April 1969, McGill Univ., Montreal, 195pp.
- Elsasser, W.M., 1942: "Heat Transfer by Infrared Radiation in the Atmosphere". Harvard Meteor. Studies No. 6, 43 pp.
- Elsasser, W.M., and M.F. Culbertson, 1960: "Atmospheric Radiation Tables". Meteor. Monogr., Vol. 4, no. 23, pp. 1-43.
- Emmons, G., 1947: "Vertical Distributions of Temperature and Humidity Over the Ocean Between Nantucket and New Jersey". Papers Phys. Oceanog. Meteor., Vol. 10, No. 3.
- Frost, B.A., 1948: "Atmospheric Turbulence". Q.J.R.M.S., Vol. 74, pp. 316-338.
- Gandin, L.S., 1969: "Objective Analysis of Meteorological Fields". Hydrometeorological Publ. House, Leningrad, 1963; Israel Program for Scientific Translations, Jerusalem, 1965, 242pp.
- Gordon, A.H., 1950: "The Ratio Between Observed Velocities of the Wind at 50 Feet and 2000 Feet over the North Atlantic". Q.J.R.M.S., Vol. 76, pp. 344-348.

- Jeffreys, H., 1920: "On the Relation Between Wind and Distribution of Pressure". Proc. Roy. Soc. (London), Vol. A96, pp. 233-249.
- Lally, G.D., 1973: "Ice Formation in the Gulf of St. Lawrence". (Unpubl. McGill M.Sc. Thesis), McGill University, Montreal.
- Lettau, H.H., Davidson, B., 1957: "Exploring the Atmosphere's First Mile". Vol. 11, "Site Description and Data Tabulation". Pergamon Press, Inc., New York.
- Mastenbrook, H.J., 1966: "Water Vapor Observations at Low, Middle and High Latitudes During 1964 and 1965". Naval Research Laboratory Report 6447, 199 pp.
- Matheson, K.M., 1967: "The Meteorological Effect on Ice in the Gulf of St. Lawrence". Publ. in Meteor., Sept. 1967, McGill Univ., Montreal, 110 pp.
- Munn, R.E., 1966: "Descriptive Micrometeorology" Advances in Geophysics, Supplement 1, Academic Press, 245 pp.
- Ninomiya, K., 1972: "Heat and Water Budget over the East China Sea in the Winter Season". J. Meteor. Soc. Japan, Vol. 50, pp. 1-16.
- Ninomiya, K., 1968: "Heat and Water Budget over the Japan Sea and the Japan Islands in Winter Season". J. Meteor. Soc. Japan, Vol. 46, pp. 343-372.
- Ninomiya, K., 1964: "Water Substance Budget over the Japanese Sea and the Japan Islands During the Period of Heavy Snow Storms". J. Meteor. Soc. Japan, Vol. 42, pp. 317-329.
- Palmén, E., Soderman, D., 1966: "Computation of the Evaporation from the Baltic Sea from the Flux of Water Vapor in the Atmosphere". Geophysica, Vol. 8, pp. 261-279.
- Reynolds, G., 1956: "A Wind Analysis for the Northern Irish Sea". Q.J.R.M.S., Vol. 82, pp. 469-480.
- Roll, H.U., 1965: "Physics of the Marine Atmosphere". International Geophysics Series, Vol. 7, Academic Press, New York, 426 pp.
- Sellers, N.D., 1969: "Physical Climatology". Univ. of Chicago Press, Chicago, 272 pp.
- Squires, P., 1958: "The Spectral Variation of Liquid Water and Droplet Concentration in Cumuli". Tellus, Vol. 10, pp. 372-380.
- Vowinckel, E., 1965: "The Energy Budget over the North Atlantic - January 1963". Publ. in Meteor., No. 105, McGill Univ., Montreal, 38pp.
- Vowinckel, E., and S. Orvig, 1972: "EBBA, An Energy Budget Programme". Publ. in Meteor., May 1972, McGill Univ., Montreal, 50 pp.

Warner, J., 1955: "The Water Content of Cumuliform Cloud". Tellus,  
Vol. 7, pp. 449-457.

Yamamoto, G., 1952: "On a Radiation Chart". Sci. Reports, Tohoku Univ.,  
Vol. 4, pp. 9-23.

Zillman, J.W., 1972: "A Study of Some Aspects of the Radiation and Heat  
Budgets of the Southern Hemisphere Oceans". Met. Study no. 26,  
Bureau of Meteorology, Dept. of the Interior A.G.P.S.,  
Canberra, Australia.